

ARISTOTLE UNIVERSITY
SCHOOL OF NATURAL SCIENCE - PHYSICS DEPARTMENT
SECTION OF ASTRONOMY, ASTROPHYSICS AND MECHANICS

Star Forming Regions in Active Galactic Nuclei with Multiwavelength Observations

Diploma Thesis
By *Lesgidou Nastazia-Lemonia*



· 2013 ·

I would like to thank my three supervisors, John Seiradakis, Marcos Trichas and Eleni Kalfountzou, for giving me the chance to cooperate with them in this exciting field, their constant contribution and their continues and patient guidance.

Abstract

The goal of this thesis is the multiwavelength study of a sample of galaxies that contain an Active Galactic Nuclei (AGN). The sample that has been used is the result of cross-correlations of different catalogs in two different regions of the sky (the *ELAIS N1* and the *Lockman Hole*). The original catalogs derive from observations with earth based and space observatories that absorb in X-ray, Radio, Infrared and Optical wavelengths and they are the followings: the *Swire Redshift Catalog* of Spitzer Space Telescope, the *FIRST Survey* and the *21 cm Survey* of VLA, the *Chandra Surveys*, the *XMM-Newton Catalog* and *GMRT observations* in 325 MHz and in 610 MHz.

Our final sample consists of 501 sources consists of starbursts $L_x < 10^{42}$ erg/s, AGN with 10^{42} erg/s $< L_x < 10^{44}$ erg/s and QSO with $L_x > 10^{44}$ erg/s. All of our sources had Optical, X-rays and Infrared counterparts and only 99 sources of our sample had radio counterparts. Based on their hard X-ray luminosity I investigated the star formation rate of the two populations (radio loud - RL, radio quiet - RQ) and the dust mass of the host galaxies of our sources. The starburst galaxies of our sample appear to have only radio quiet sources, which is in agreement with the *spin paradigm* (Blandford, 1990; Wilson and Colbert, 1995). The AGN sources of our sample have both radio quiet and radio loud sources and the radio loud sources appear to have higher average star formation rate and dust mass which could be supported by the jet-induced star-formation (*positive feedback*) idea. In the QSO sample we cannot distinguish a difference between the RL and RQ populations. However this could be a result of the small number of radio quiet sources that we have in our radio detected sample.

Contents

Chapter 1

Introduction	10
1.1 Galaxies.....	10
1.1.1 Elliptical Galaxies	11
1.1.2 Spiral Galaxies.....	12
1.1.3 Irregular Galaxies	12
1.1.4 Active galaxies	12
1.2 Starburst Galaxies	13
1.3 Introduction to Active Galactic Nuclei.....	15
1.3.1 Brief history	15
1.3.2 AGN Structure	17
1.3.3 AGN Emission Process.....	17
1.3.4 The Unified Model.....	20
1.3.4.1 Seyfert Galaxies	21
1.3.4.2 Low-Ionization Nuclear Emission-Line Region galaxies.....	21
1.3.4.3 Quasars	22
1.3.4.4 Blazars.....	22
1.4 The AGN Spectra Properties.....	23
1.4.1 Radio Properties	25
1.4.2 Infrared Properties	26
1.4.3 Optical Properties	27
1.4.4 X-ray Properties.....	27

Chapter 2

Starburst co-evolution	29
2.1 AGN-Starburst Connection, why we believe there is a connection	29
2.2 Co-evolution of AGN and Star Formation Rate Density	30
2.3 Models to Explain the Co-evolution	31
2.4 Support of the Merger Model.....	37
2.5 Problems with the Merger Model.....	38

Chapter 3

Sample Selection	40
3.1 The Spitzer Space Telescope (SST)	41
3.1.1 SWIRE Redshift Catalog.....	42
3.1.2 SWIRE ELAIS-N1 Infrared.....	44
3.1.3 SWIRE ELAIS-N1 optical	44
3.2 Chandra Space Telescope	44
3.2.1 Chandra ELAIS-N1 survey.....	46
3.2.2 The SWIRE/Chandra Survey: The X-ray Sources.....	47
3.3 Giant Metrewave Radio Telescope	48
3.3.1 325-MHz Observations of the ELAIS-N1 field	48
3.3.2 610-MHz Observations of the ELAIS-N1 field	49
3.4 Very Large Array - VLA	50
3.4.1 VLA First Survey.....	51
3.4.2 Deep VLA Survey at 20 cm	52
3.5 Isaac Newton telescope	53
3.5.1 XMM-Newton catalog of the Lockman Hole	53
3.6 The Final Sample and Properties	54

Chapter 4

Sample Analysis	58
4.1 Radio loud- Radio quiet division	58
4.2 Star Formation Rate	63
4.3 The Infrared Continuum	66

Chapter 5

Results – Conclusions	69
5.1 Mergers and Triggering of Activity.....	70
5.2 AGN feedback	71
5.3 Host galaxies	72
5.4 Conclusions.....	75
References	76

Table of Figures

Figure 1.1.— Hubbles “Tuning Fork”, On the left side of the sketch, the handle of the fork consists of elliptical galaxies from E0 to E7 (0-7 are the degrees of flatness). Each tine of the fork consists of the two classes of spiral type, the lower tine represents the spirals that contain a bar component and the upper the normal spirals. A graphic representation by NASA. 11

..... 14

Figure 1.2b.— A multiwavelength view of the starburst galaxy M82 (NASA). 14

Figure 1.3.—This image is a radio map of the radio galaxy Cygnus A. It have been produced by observation at a wavelength of 6cm at the Very Large Array, by John Conway and Philip Blanco in March 1994. 16

Figure 1.4.—This figure is a visual depiction of the effect of a large mass on the fabric of spacetime. Furthermore there is comparison of how objects with lower density, as the sun, a white dwarf and a neutron star, can affect the spacetime fabric. 17

Figure 1.5.—The unified model of AGN, all share a common structure though appear different because of the different angle at which they are observed (illustration: Sonoma State University). 20

Figure 1.6.- the electromagnetic spectrum (NASA). 23

Figure 1.7.—The “Whirlpool Galaxy” (Messier 51), a spiral galaxy that interacts gravitationally with a smaller companion galaxy. In the left there is the X-ray picture obtained with Chandra, in the center up the visible picture tobtained with T&D Hallas, in the center down there is the far-infrared picture taken by IRAS, in the right up the mid infrared one taken by ISO and finally down in the right the radio picture taken by VLA (<http://coolcosmos.ipac.caltech.edu>) 24

Figure 1.8.—A VLA image of the galaxy M87 radio galaxy. The galaxy’s super massive black hole lies within the bright, reddish region. The image was made at a radio wavelength of 900 cm (NRAO/AUI and F.N. Owen, J.A Eilek, N.E Kassim). 25

Figure 1.9.- A Mid Infrared image of the starburst galaxy M82 obtained with the IRAS (Infrared Astronomical Satellite) (<http://coolcosmos.ipac.caltech.edu>). 26

Figure 1.10.- A powerful radio source known as Centaurus A (NGC 5128) Image obtained with AAO. 27

..... 27

Figure 1.11.- This is M82 a 11 million light years distant starburst galaxy. The bright spots in the middle of the picture are supernova remnants and X-ray binaries whom x-ray luminosity suggests a black hole in the center of the galaxy. This image is obtained by Chandra (<http://chandra.harvard.edu>). 28

..... 28

Figure 2.0.— The Star Formation Rate density data used in defining the best fitting parametric forms and the resulting fits (Hopkins & Beacom 2006). 30

Figure 2.1—The AGN density as a function of redshift in a range of luminosity classes.(Hasinger et al.2005). 31

Figure 2.2.—At the top a representation of the distribution of dark matter at zero redshift and at the bottom a representation of galaxy light for a thickness of 15 h-1Mpc. This is a result of Croton et al. 2006 by using the Millennium Run. For the figure in the top the color encodes the local velocity dispersion and the intensity the surface density and for the bottom figure intensity encodes the surface brightness and the color the mean B-V color (Croton et al.2006). 33

Figure 2.3.—The star formation rate density as a function of redshift. The solid line represents the model that is in agreement with observations. In this model galaxies form a part of their total mass relatively early (Croton et al.2006). 34

Figure 2.4.— The Hopkins merger model. The gas inflows trigger the supermassive black hole’s accretion and starbursts. The dust and gas clouds make the AGN obscured. Then the AGN feedback sweeps away the gas clouds and as a result it causes star formation and black hole accretion (Hopkins et al.2006) 35

Table of contents

Figure 2.5— The star formation rate density as a function of redshift by the star formation model of Hopkins et al. 2006. The results come from the quasar luminosity function considering an average disk gas fraction :

$$f_{\text{gas}} = 10^{\frac{-t}{t_H}} = e^{-\frac{t}{6\text{Gyr}}}$$

The shaded area represents the 1σ range allowed. The dot-dashed line and dashed lines shows the result that occur assuming that the disk gas fraction is constant with values: $f_{\text{gas}} = 1.0$ and $f_{\text{gas}} = 0.1$.

The dotted lines represent the result from Hopkins & Beacom (2006) observations.	36
Figure 2.6a—Luminosity function for both DEEP2 All and Red galaxy samples versus magnitude. The triangles are strict upper limits to the galaxies' density under the assumption that all failed-redshift red galaxies are located only in that bin. (Willmer et al.2006).	37
Figure 2.7.—Rest frame U-B color against B-band absolute magnitude. The Blue dots represent the DEEP2 galaxies and the red dots the X-ray sources, Squares indicate hard X-ray sources, larger dots indicate more luminous systems. The dashed line shows the limits between red and blue galaxies (Nandra et al.2007).....	39
Figure 3.1.—An artist's conception about Spitzer space telescope (Nasa).....	41
Figure 3.2.— The SWIRE Survey Fields are shown in red. The contour levels in blue, green yellow are respectively 1, 2, 4 MJy/sr.	42
Figure 3.3.—An artists conception of Chandra Space Telescope (Nasa).....	45
Figure 3.4.— Illustration of Chandra's elliptical orbit (http://chandra.harvard.edu).....	46
Figure 3.5.—A picture of GMRT taken in January 2001.....	48
Figure 3.6.— In the left a picture of VLA as seen from the north, in the right a close-up picture of one of VLA's dishes (http://www.vla.nrao.edu/).....	50
Figure 3.7.- The northern sky coverage of the survey. The different colors represent the different years that survey had been held.	51
Figure 3.8.- The southern sky coverage of the survey. The different colors represent the different years that survey had been held.	52
Figure 3.9.— A photograph of the Isaac Newton Telescope (http://www.ing.iac.es/).	53
Figure 3.10.- hard X-ray luminosity in erg/sec versus redshift. The sources have been divided in 3 categories the normal starbursts (non AGN) with $L_x < 10^{42}$ erg/s are presented with a grey color, the starburst dominated AGN galaxies with $10^{42} < L_x < 10^{44}$ erg/s with a green color and QSO's with $L_x > 10^{44}$ erg/s and a blue color.....	55
Figure 3.11.-Radio luminosity in watts versus redshift for the 99 detected sources with a radio counterpart.....	56
Figure 4.1.— Redshift versus the logarithm of hard x-ray luminosity. The sources are divided to radio loud with the red color, radio quiet with the blue color. The black line represents the division of starbursts ($L_x < 10^{42}$ erg/s) and AGN ($10^{42} < L_x < 10^{44}$ erg/s). The grey line divides the sources in AGN and QSOs ($L_x > 10^{44}$ erg/s).....	59
Figure 4.2.- A Histogram of the logarithmic radio luminosity (in watts) of our detected sources. With the red color we represent the radio loud sources of our sample and with the blue dotted line the radio quiet sources.....	60
Figure 4.3a.— A histogram of radio loudness. The black line represents the QSO population, the black dotted line the AGN and the blue the starbursts. The grey line is the radio loudness limit, a source with $R < 1$ is radio quiet and a source $R > 1$ is radio loud. In this Histogram we have both radio detected and undetected sources.....	61
Figure 4.3b.- A histogram of radio loudness. The black line represents the QSO population, the black dotted line the AGN and the blue line the starbursts. The grey line is the radio loudness limit, a source with $R < 1$ is radio quiet and a source $R > 1$ is radio loud. In this Histogram we have only radio detected sources.	62
Figure 4.4.-A histogram of the star formation rate in $M_{\text{sun}}/\text{year}$. With the black dotted line are shown our undetected sources, the blue represents the radio quiet detected sources and red the radio loud detected sources.	64
Figure 4.6.- A histogram of the IR luminosity divided by the optical luminosity. Our undetected sample is represented with the grey color, the red shows our detected radio loud sources and respectively the blue corresponds to our detected radio quiet sample.....	66
Figure 4.7.- In this figure we present the logarithmic hard X-ray luminosity counted in erg/sec versus the logarithmic M_{dust} counted in M_{sun} (solar masses). With the blue dots we have the radio quiet radio detected sources of our sample accordingly with the red dots.	67

Table of contents

Figure 4.7.- *A histogram of the logarithmic dust mass of AGN's host galaxy counted in solar masses. With the blue color we have the radio quiet detected objects of our sample, the red shows the radio loud detected ones and the grey the undetected.*..... 68

Figure 5.1.-*The logarithmic X-ray luminosity in erg/sec versus the logarithmic star formation rate in $M_{sun}/year$. With the blue dots we show the radio quiet radio detected sources and with the red ones the radio loud radio detected sources of our sample. With the blue circles we present the mean values of the radio quiet detected sample and with the red circles the mean value of the radio loud detected one We have placed the mean values in the center of the three classes (starburst, AGN, QSOs). Furthermore with the blue and red straight line we can see the errors.* 72

Figure 5.2.-*The logarithmic X-ray luminosity in erg/sec versus the logarithmic M_{dust} dust mass of the host galaxy in M_{sun} . With the blue dots we show the radio quiet radio detected sources and with the red ones the radio loud radio detected sources of our sample. With the blue circles we present the mean values of the radio quiet detected sample and with the red circles the mean value of the radio loud detected one We have placed the mean values in the center of the three classes (starburst, AGN, QSOs). Furthermore with the blue and red straight line we can see the errors.*..... 74

List of Tables

Table 3.1.— *The first column is the field name, the second is right ascension, next is the Declination of the field center, the forth is the infrared background emission at 100 μ m band fifth is the color excess E(B-V) and the last one is the size in square degrees.* 43

Table 3.2.— *The first column of table 1 describes the name of the Chandra Survey. The second records the observation lds that have been used. The next is the exposure time in ks. The forth column describes the total surveyed area in deg², and the last column gives the total number of sources in each survey.* 47

Table 3.3.—*The observation summary of S. K. Sirothia et al. 2008.*..... 49

Chapter 1

Introduction

In this general introduction chapter I analyze some basic astronomical concepts that will help the reader understand the nature and physics of an AGN. First, I present some general information about galaxies and their classification. Moreover, I present a general introduction to starburst galaxies and AGN. Finally, I give a thorough introduction to AGN that contains a brief history, a presentation of the unified model, a discussion of its structure and its spectra properties.

1.1 Galaxies

Galaxies are massive, gravitationally bound structures that consist of millions of star and stellar remnants. In 1926 Edwin Hubble using the largest until then telescope in the world, the 2.5m Hooker telescope at Mount Wilson was trying to study individual stars within M31, the great spiral nebula in Andromeda, this led to the discovery and the first classification of galaxies into two classes depending their shape and morphology, the spiral and the elliptical galaxies. It wasn't too long before Hubble identified an extra intermediate class S0 that looked smooth like an elliptical galaxy but was flat as a spiral. He also presented all these types in a diagram (Figure 1.1) which is still very useful in the classification of galaxies.

Today we divide galaxies into three distinct classes which reflect distinct physical properties: the Elliptical, Spiral and irregular galaxies.

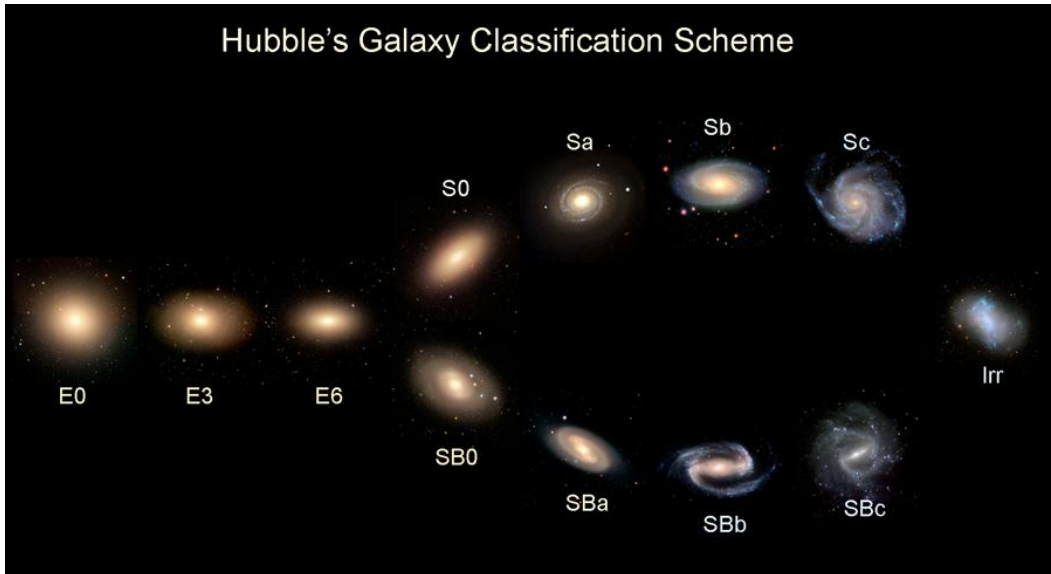


Figure 1.1.— Hubbles “Tuning Fork”, On the left side of the sketch, the handle of the fork consists of elliptical galaxies from E0 to E7 (0-7 are the degrees of flatness). Each tine of the fork consists of the two classes of spiral type, the lower tine represents the spirals that contain a bar component and the upper the normal spirals. A graphic representation by Nasa.

1.1.1 Elliptical Galaxies

The elliptical galaxies are characterized by their elliptical isophote shapes, the light intensity in the edge of the ellipse is equal. Their number range from hundreds of millions to over one trillion stars. They are believed to constitute approximately 10-15% of galaxies in the local group. They are most likely to be found to the centers of galaxy clusters. Some other characteristics are their masses that range from about 10^7 up to 10^{13} solar masses and their diameters that range from about 1/10 kpc up to about 100kpc. E galaxies ellipticities are given from the following equation:

$$\varepsilon = 1 - \frac{b}{a}$$

Where b stands for the minor axis and a the major.

The ellipticities of the elliptical galaxies range between 0 and 7, which is the main characteristic that divides E galaxies into subclasses:

$$En, \text{ where } n = 10\varepsilon$$

Thus, a very round E galaxy is classified as E0; on the contrary the galaxy with the largest observed ellipticity is classified as E7.

E galaxies consist of an old, low-mass star population few young stars and few open star clusters. This is the reason why in E galaxies' observations the red color

dominates. The stellar color can be better understood by the blackbody radiation. Thus, the variety of stellar colors that we observe is the direct consequence of their surface temperatures. The spectra of stars are very similar to blackbody radiation curves of various temperatures that range from about 1000 to 50000 Kelvin. Generally, E galaxies have minimal star formation activity due to the lack of interstellar mass (gas and dust).

1.1.2 Spiral Galaxies

The spiral or disk galaxies are more complex objects than the elliptical galaxies but much more common to be found in the universe since they make up the 60% of the total number. They appear as a rotating disk with two spiral arms that extend from the center of the disk, a near-spherical halo of stars and a supermassive black hole at the center of the central bulge. The spiral galaxies are divided in three categories according to how tightly the spiral arms are wrapped. The most tightly would belong to class Sa and the least tightly bound to Sc. Most of the spiral galaxies apart from their disk component have also a central bulge component. Spiral arms unlike bulges tend to consist of young star clusters, thus, they appear blue in observations. Another classification of spiral galaxies is whether they have a bar component. This is the characteristic that gives the two tines of the tuning fork where the lower tine represents the galaxies with a bar component and the upper represents the ones without one. Observations of barred galaxies show that bars are most likely to be found in the plane of the disk. Spiral galaxies are mostly found in low-density regions and have greater star formation activity than the elliptical ones. The range of mass for the spiral galaxies is 10^9 - 10^{12} solar masses while the typical diameter of the visible disk range in between 5-100kpc.

1.1.3 Irregular Galaxies

Irregular galaxies have not a distinct shape like spirals or ellipticals. They don't belong to any of the Hubble's classes and cannot be distinguished or classified according to their morphology due to the fact that they don't have many common characteristics. They usually appear as large clouds of dust, gas and stars. They are divided in two categories, in the irregulars type I, the galaxies that have a high star formation rate, and the irregulars type II, the ones with a low star formation rate.

1.1.4 Active galaxies

Apart from the galaxy classification according to their morphology and shape, we can categorize galaxies according to their core activity. Generally, an active galaxy is a galaxy with a high Luminosity, strong emission lines, nonthermal spectra and a very bright core compared to the rest of the galaxy.

Active galaxies can take two different forms- The galaxies that are active due to the radiation from their recently formed stars and the galaxies whose spectra are dominated by non-stellar energy sources (nonthermal radiation).

1.2 Starburst Galaxies

A starburst galaxy is a galaxy with a far more intense radiation that originates from star formation than a normal galaxy but unfortunately there isn't a sharp transition between a normal and a starburst galaxy (Figure 1.2). The starburst region in most cases is placed in the center of the galaxy and it constitutes approximately the 10% of the total galaxy (with a typical radius of 100-1000pc). Despite their rather small size starbursts are converting gas into massive stars at a rate 100-1000 times faster than in a normal galaxy like our own. The starburst galaxy is usually formed from the collision of many smaller star-forming regions. Some of them have even reached the HII region stage, thus, a characteristic of a starburst galaxy is the existence of emission lines of HII regions (lines due to hydrogen and helium plus forbidden lines from singly ionized oxygen and nitrogen).

The luminosity of a starburst galaxy, as mentioned above, is extremely high. However during the early stages of the universe the contribution of starburst galaxies to the complete star production it is estimated that it was even higher (Christopher R. Kitchin – 2007). There is a number of suggested triggering mechanisms that include interactions and mergers (Schweizer 1987; Jog & Das 1992), bar instabilities (Shlosman et al. 1990) and kinematic effects from stellar winds (Heckman et al.1990). The most important triggering mechanism seems to be the gravitational interactions between galaxies. Stellar winds and supernovae heats the interstellar gas and it expands along the lines of least resistance which is perpendicular to the galaxy's disk. As a result, the galactic winds that are created can reach very high temperatures (several million Kelvin) and speeds up to a thousand kilometers per second.

Starburst galaxies can be located at all distances, which indicates that starburst galaxies have been created from the beginning of the universe until now. The observation of a large number of galaxies with intense star-formation at a high redshift suggests that starburst galaxies were a dominant phase of early galaxy evolution (Steidel et al. 1996, Lowenthal et al. 1997). Generally starbursts feature a very large amount of cool molecular gas (up to 100 pc) in which there are star forming regions like cocoons. Despite these cocoons are the largest structures found in the whole Galaxy, they have just been discovered recently. They radiate in the far infrared and microwave regions of the spectrum, thus their temperature is quite low as 10K (-263°C). Their average density is approximately a billion molecules and atoms per cubic meter. The very low temperature and high concentrations of the material in these regions is the reason of triggering the gravitationally collapse and eventually the production of newborn stars.

There are two models that explain this phenomenon. The first one is called "gravitational collapse and fragmentation"(Arreaga-Garcia et al.2007) and it is referred to the collapsing clouds that due to their very large size they fragment during the infall so that many binary and multiple stars are created. The second model is called "competitive accretion", according to it as the clumps collapse several centers are created, each about 0.3pc. Finally the centers themselves collapse under gravity and form starburst cocoons.



Figure 1.2b.— A multiwavelength view of the starburst galaxy M82 (NASA).

1.3 Introduction to Active Galactic Nuclei

In this section I am going to present a brief history of AGN and then I will briefly analyze their structure. Moreover, I am going to mention the most popular AGN categorization which is according to their observation angle. According to the unified model we observe different kinds of active galaxies just because we observe them in a different angle. For example in Seyfert galaxies we are looking either the edge of the disk or at an inclined angle, so we categorize them to two populations. Likewise in the BL Lac objects we look directly into the jet. Finally when we observe a Quasar we see extremely bright objects because they are the cores of galaxies with extremely massive black holes, the 4 types of galaxies are represented in *Figure 1.4*.

1.3.1 Brief history

One of the ultimate aims of astronomy is to understand how the universe was formed. Because of that quest, scientists have been searching for centuries the answer to how galaxies were created. The study of Active Galactic Nuclei can bring the scientific society closer to the answers that they seek.

The story of AGN research begun in 1909, when Edward Fath (Steppins & Fath 1906, Fath 1909&1910) was to determine whether spiral nebulae consisted from stars or they were gaseous objects. Among the nebulae that he was studying was NGC 1068, that unlike the most objects of his studies, it had both bright and absorption lines. Slipher in 1917 (Slipher 1917) found that the bright and dark lines of NGC spectra were emission lines of small disks.

After that observation nuclear emission lines were found in other nebulae, but the answers came with the research paper of Carl Keenan Seyfert in 1943. Seyfert studied the spectrograms of six galaxies that had bright emission lines. He attributed those emission lines on strong Doppler broadening. This indicates very high velocities, from 500 to 4000 km/s. These galaxies with the very bright emission lines are now called Seyfert galaxies.

A few years before Seyfert studies Carl Jansky, in 1931, constructing the first radio telescope and after some systematic observations from all the directions, he came to some conclusions. He observed a static from thunderstorms, and a steady periodic static of unknown origin. At first he associated this static with the sun, but after he continued his measurements he came to the conclusion that this steady noise was coming from the center of the Milky Way galaxy. Jansky's studies triggered the development of the radio astronomy research through all over the world and that was the beginning of an era that led to AGNs.

One of the most important steps for the AGN studies was the accidental discovery of a small source in Cygnus. Bolton and Stanley in 1948 with studies in Cygnus managed to prove using a sea-cliff interferometer that the origins of the steady noise that Jansky discovered probably didn't have a thermal origin. In the same year Bolton published a catalog with six sources with discrete nature. From that point many other objects were identified. One of those sources was Cyg A (*Figure 1.3*), an object with peculiar morphology.

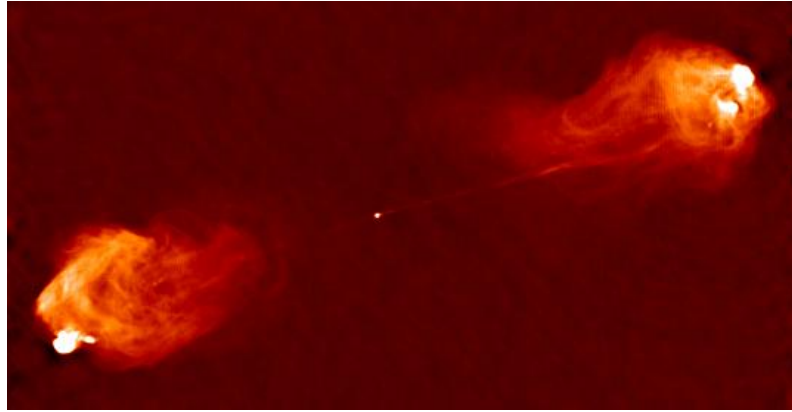


Figure 1.3 .—This image is a radio map of the radio galaxy Cygnus A. It have been produced by observation at a wavelength of 6cm at the Very Large Array, by John Conway and Philip Blanco in March 1994.

In order to proceed to a thoroughly identification, Baade and Minkowski measured the distance of Cygnus A using the giant 200-inch reflector at Palomar Observatory and the redshift method. The redshift of the object implied a very large distance, approximately 31 Mpc (for Hubble constant $H_0=540\text{km/s/Mpc}$) which implied an enormous luminosity. Reber gave the explanation that the emission lines were created by ionized gas in the interstellar medium.

The explanation for the enormous luminosity was given by Alfvén and Herlofson with their research paper at 1950. They suggested that the emission wasn't thermal but it was synchrotron emission which can explain the enormous amounts of energy that were observed. In the two following decades many radio searches had been held and a great number of sources were identified.

The breakthrough came with the discovery of quasars, or quasi-stellar radio sources (QSRS). In 1960, Sandage observed an object with a spectrum with very strange emission lines that were indicating energetic processes, at not familiar wavelengths. The images that Sandage obtained shown an object quite similar to a normal star. This was the prevalent explanation until 1963, when Hazard, Mackey and Shimmins observing a lunar occultation of the quasar 3C 273, they realized that the quasar consisted from two other objects. The two objects had different spectrum and from the disappear and reappear time of the lunar occultation it became clear that they were separated by 20 seconds.

After a closer look to the spectra of the quasar 3C 273, Schmidt realized that these strange emission lines were actually spectral lines of hydrogen redshifted at a rate of 15,8%. Finally he came to the conclusion that 3C 273 couldn't be a star. Many other quasars were observed the following years. The mystery of the quasar's spectra was solved with the measurement of the redshift. All those objects looked like stars but their redshifts indicated enormous distances from our planet. A few years later astronomers divided quasars in two categories- the *radio loud* and the *radio quiet* quasars. In total the 10% of quasars are radio loud and the 90% radio quiet. Today there are about 12000 quasars known.

1.3.2 AGN Structure

The observational fact that established the structure model of AGN was the enormous x-ray luminosities that was observed to QSOs $L_x \leq 10^{46}$ erg/s while until then the higher x-ray luminosities known were the ones from binary stars ($L_x \leq 10^{37}$ erg/sec) and supernova remnants ($L_x \leq 10^{35}$ erg/s). This fact indicated that there had to be a mechanism that would have as a central engine a very large and efficient source of energy that would be able to fuel this enormous energy output of these objects. With their paper in 1993 Lawrence & Papadakis made the conclusion that the mechanism that fueled these objects couldn't be a stellar process. The black hole hypothesis was made after the determination of some other common characteristics of AGN, all of these objects show instability in their flux and the energy that they emit. Also, as mentioned above, AGN's optical spectrum is dominated by strong emission lines. Another characteristic of a galaxy with an active galactic nucleus is that there is an ejection of material at very high velocities from the center of the galaxy, in the form of two jets with an opposite direction that can reach up to millions of light years which makes them very detectable.

1.3.3 AGN Emission Process

The existence of black holes in the center of galaxies is a rather recent assumption. Their sizes vary from a black hole the size of our sun to a super-massive black hole almost the size of a dwarf galaxy (approximately $10^9 M_{\text{sun}}$). Due to its enormous density, a black hole creates a space time dent (Figure 1.4). A dent, as Albert Einstein predicted with his theory of general relativity, affects the movement of matter falling into the black hole. It is invisible, but astronomers deduced its existence after detecting two x-ray frequencies from a black hole, that were identical to emissions noted nine years ago.

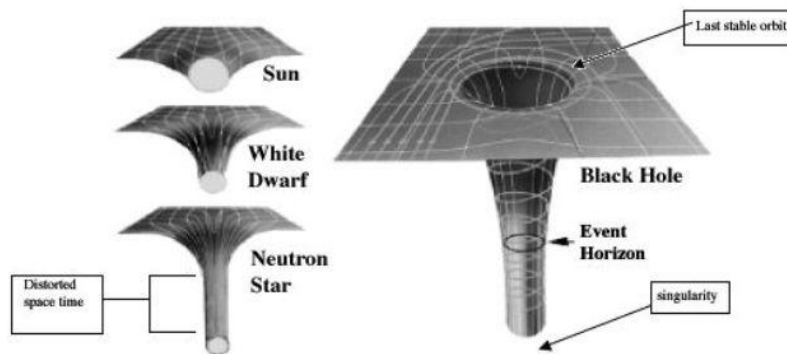


Figure 1.4.—This figure is a visual depiction of the effect of a large mass on the fabric of spacetime. Furthermore there is comparison of how objects with lower density, as the sun, a white dwarf and a neutron star, can affect the spacetime fabric.

Chapter 1- Introduction

Even if there is an enormous magnitude difference between black holes, they all can be described by their mass, their spin and their charge. The properties of a black hole are expressed by using the gravitational radius r_g and the Schwarzschild radius¹ r_s .

$$r_g = \frac{GM}{C^2}, r_s = 2r_g \quad (1) \quad (\text{Schwarzschild 1916})$$

In 1963 it was first proposed by Kerr the uncharged, spinning mass of the black hole. Thus it is necessary for the description of a black hole to mention the angular momentum s :

$$s \approx I\Omega \approx \frac{Mr^2\omega}{r} \approx Mr_{gc} \quad (2)$$

where Ω is the angular velocity of the black hole. The angular momentum per mass is the following :

$$s/M = ac \approx r_g c \approx 5 * 10^{23} M_g cm^2 / s \quad (3)$$

On the other hand, the limit of the maximum luminosity attainable for an AGN engine before it loses mass by radiation pressure is:

$$L_{EDD} = \frac{4pGMcm_H}{\sigma_T} = 1.25 \times 10^{38} \text{ erg} \times s^{-1} \left(\frac{M}{M_{sun}} \right)$$

Where m_H is the mass of a hydrogen atom and σ_T is the Tompson cross-section of an electron. The mass of a black hole according to the measured luminosities can be predicted at 10^6 - $10^9 M_{sun}$. Due to the fact that this mass has to be extremely dense the only engine that can describe successfully an AGN is a black hole in its center.

The process that takes place in a black hole that empowers the black hole and converts the gas material that surround the black hole to jets is the mechanism of an accretion disk.

¹ **Schwarzschild radius:** The radius, according to the general theory of relativity, at which is compressed all the mass of the object when the escape speed from the surface is equal to the speed of light. The Gass matter that surrounds the black hole can be inevitably drawn into it, if it crosses the Schwarzschild radius. The escape speed of the BH is given by Newton's equation: $V_{esc} = (2GM/R)^{1/2}$. The SR is equal to the speed of light, so even light cannot escape from the inner side of a black hole.

Chapter 1- Introduction

When gas flowing in towards a central object it appears to have an angular momentum so it doesn't reach the object directly. The movement and the orientation of the accretion disk depends on the angular momentum. In order for the material to reach the black hole there has to be a form of friction. In our case the friction that is needed has been provided by the magnetic forces in the ionized plasma.

The outflows from accretion disks may be related to a different observational and theoretical model. Different objects in the universe have different outflows. For example, young stars show powerful outflows unlike the older population .The outflows of massive black holes are collimated jets.

Recent numerical simulations of magnetized accreting plasma in General Relativity, has clarified the possible origin of the jets. Simulations reveal that the jets emerge self-consistently from the accretion flow. If the black hole rotates with a higher angular velocity , then the outflow is stronger and more energetic.

However , there are scientists that support the theory that a part from the energy from the outflow , comes directly from the rotational energy of the black hole rather than from the accreting matter. This possibility has been discussed for 30 years, but still there are not observational evidence that agree with it.

To summarize a galactic nucleus is active if it generates a substantial amount of energy by unique processes comparing the other edges of the universe. The accepted model of an active galactic nucleus consists from a rotating super-massive black hole in the center of the galaxy that creates a dense disk of material that is falling in the black hole, an accretion disk. The inflowing gas matter due to it's angular momentum ends up rotating very rapidly as it approaches the black hole. This accretion due to the friction among the gas matter is accompanied by enormous release of radiative energy, the jets (Figure 1.5).

1.3.4 The Unified Model

At 1993 Antonucci, being influenced by some spectropolarimetry observations of a sample of Seyfert galaxies that indicated the presence of weak, broad, permitted emission lines (Antonucci & Miller 1985; Miller & Goodrich 1990), presented the “unified model”. According to which, different types of AGN can be understood as a single object that is observed from a different angle (Figure 1.5). This theory was further explored by Urry & Padovani 1995. According to the latest theories for AGN structure, there is a torus of gas and dust around the central engine (black hole-accretion disk), thus the central region can be obscured if the direct line-of-sight would pass through this torus. The broad line region, the region that produces the broad permitted line, is thought to be quite close to the central engine, as a result to that it can be easily obscured. Thus we can categorize AGN to the following classes, according to the angle of the observer:

- Seyfert Galaxies
- Low-Ionization Nuclear Emission-Line Region galaxies (Liner Galaxies)
- Quasi-Stellar Objects (quasars)
- Blazars

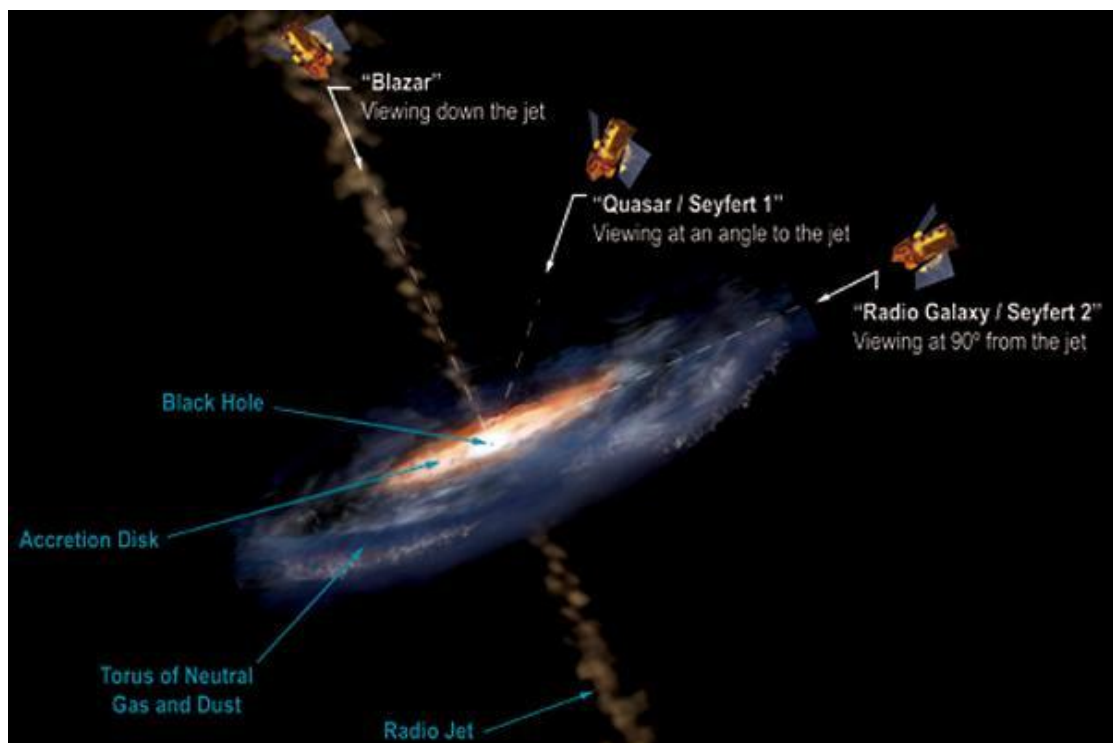


Figure 1.5.—The unified model of AGN, all share a common structure though appear different because of the different angle at which they are observed (illustration: Sonoma State University).

1.3.4.1 Seyfert Galaxies

A Seyfert galaxy, as every active galaxy has a very unusual nuclear brightness and nuclear spectra. Seyferts have an intermediate level of activity and most of them are spiral galaxies most likely barred types. The most tightly wound are much more powerful than Liner Galaxies but less powerful than Quasars. It appears that Seyferts are much closer to earth than quasars and blazars (Pringle et al. 1999; Kinney et al. 2000).

Some common characteristics of Seyferts are that they have very bright ultraviolet and x-ray emission and unusual far-infrared colors. Seyfert galaxies are low-energy gamma-ray sources. Their spectra show emission lines unusually strong and wide. As it is already mentioned above, Seyfert galaxies are divided into two classes the type-1 and type-2 Seyferts. The galaxies that belong in the type-1 class have very wide hydrogen and other allowed lines that correspond to Doppler broadening velocities of up to 10000km/s and much narrower forbidden lines, corresponding to velocities of up to 1000km/s. Type 1 Seyferts, like Broad Line Radio Galaxies and type 1 Quasars are objects that we are able to see directly into the central regions. On the other hand, type-2 Seyferts have emission lines with similar widths, corresponding to Doppler broadening velocities of 1,000km/s. The second type of Seyferts are more common than the first one and like narrow line radio galaxies and type 2 Quasars are referring to AGN that we observe at the plane of the disk.

The structure of the central regions of Seyferts is a gravitational field of a supermassive black hole 10^6 - $10^9 M_{\text{sun}}$ that creates a luminous accretion disk. The energy engine production is being held in a rather small radius, a few light days or weeks in comparison with the region of slower moving clouds that extends out a few hundred to a few thousand light years. Seyferts are found more commonly in reasonably luminous early-type spirals especially in objects that have asymmetric gravitational field, arising from a bar or induced by a nearby companion galaxy.

1.3.4.2 Low-Ionization Nuclear Emission-Line Region galaxies

LINER Galaxies

A LINER galaxy is quite common; they constitute approximately the 30-40% of the total number of AGNs (Kim et al. 1995). The majority of LINERs are early type Spirals with a bulge populations quite similar to those of normal spiral and elliptical galaxies. A LINER galaxy's spectrum is very similar to the Seyfert 2 galaxies apart from the low-ionization lines (e.g [O_I] and [N_{II}]) that are presented stronger, there is a strong emission line due to neutral oxygen, but all the other emission lines are presented weaker. The class of LINERs is a very low nuclear-luminosity class of galaxies that was identified by Heckman (Heckman 1980). They are radio quiet galaxies with a radio luminosity that are similar to the normal galaxies luminosity. Generally, they are more active than starburst galaxies but less active than Seyferts.

1.3.4.3 Quasars

Quasars are very high energy sources. The majority of them are stronger radio sources than normal galaxies and some of them even have beams of high energy and accelerate. That's the reason why the most of the high radiation energy doesn't reach us. The radio emission from quasar galaxies' jets is almost always bipolar. The 90% of those objects are radio-quiet and are called Quasi-Stellar Objects, or QSOs, the other 10% that are radio-loud are called just quasars.

In the radio spectrum, the degree of radio loudness is based on the radio emission in the form of core emission, jets and lobes. AGN can be divided in two classes, the *radio-loud* and *radio-quiet* class, according to the 'radio-loudness' parameter R_L (Ivezic et al.2002) which is defined as the logarithmic ratio of radio flux at 5GHz and optical spectral flux in the B band, centered on the wavelength $\lambda=2200 \text{ \AA}$:

$$R_L = \log \left(\frac{f_{5GHz}}{f_B} \right)$$

The established borderline for the categorization of radio-loud and radio-quiet objects is $R=1$, Radio-loud galaxies when $R \geq 1$ and radio-quiet when $R < 1$ (Kellermann et al.1989). This AGN dichotomy has been suggested due to the fact that roughly the 5%-10% of the whole AGN population are radio loud sources (Kellermann et al.1989; Ivezic et al.2002, White et al.2007). The radio-loudness may be related in some way to the host galaxy type (Smith et al.1986) or to the black hole's spin (Blandford 1990; Wilson and Colbert 1995). A big number from the radio loud population are elliptical galaxies with giant radio lobes that grow and extend from the host galaxy out to Mpc scales while releasing highly collimated jets. They also tend to have a very broad Balmer line in their optical spectra. Contrary radio quiet galaxies are more often found in spiral galaxies and have lower luminosities. However this radio bimodality is still under debate, the sharp separation into the two radio populations has been questioned following the results of the FIRST survey (Brinmann et al. 2000, White et al. 2000). Although this lack of bimodality in the FIRST (Becker, Hlefang & White 1995) data sources, according to Laor 2003, could be a result of insensitivity of the survey to the extended emission.

1.3.4.4 Blazars

Blazars are quite similar to quasars but with very weak emission lines. Blazar is an informal term used to describe the prototypical named objects BL Lacertae as well as the optically violently variable quasars. Their properties became clear when astronomers understood that the one relativistic jet of the object was pointing towards our view of sight (Figure 1.5)

1.4 The AGN Spectra Properties

The selection of multiwavelength surveys is the most efficient choice to study AGN since they appear quite different in the different parts of the electromagnetic spectrum (Figure 1.6). An example of an image in different wavelengths is given in *Figure 1.7* that depicts a spiral galaxy in X-ray, Visible, Mid Infrared, Far Infrared and Radio. Generally, AGN are some of the extragalactic emitters of very high energy in the most parts of the electromagnetic spectrum. Thus, due to the fact that AGN emission at different wavelengths is strongly correlated, multiwavelength studies can enlighten the often blur AGN research field. In this subsection I am going to discuss the different properties of AGN in the different parts of the electromagnetic spectrum. However there are some common AGN properties that correspond to all the electromagnetic spectrum. All AGN have emission of radiation over the entire electromagnetic spectrum with bolometric luminosities $L > 10^{42}$ erg s⁻¹. Furthermore the AGN spectra have non-thermal origin through all the electromagnetic spectrum.

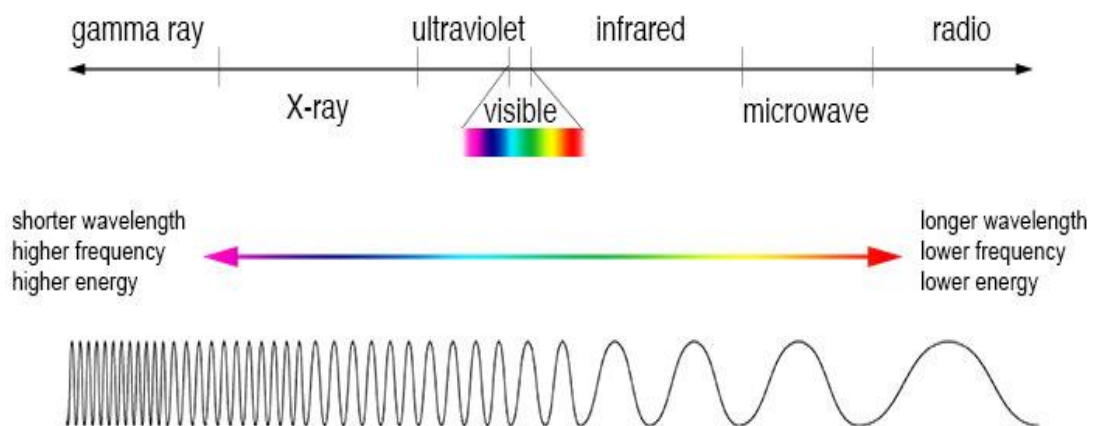


Figure 1.6.- the electromagnetic spectrum (Nasa).

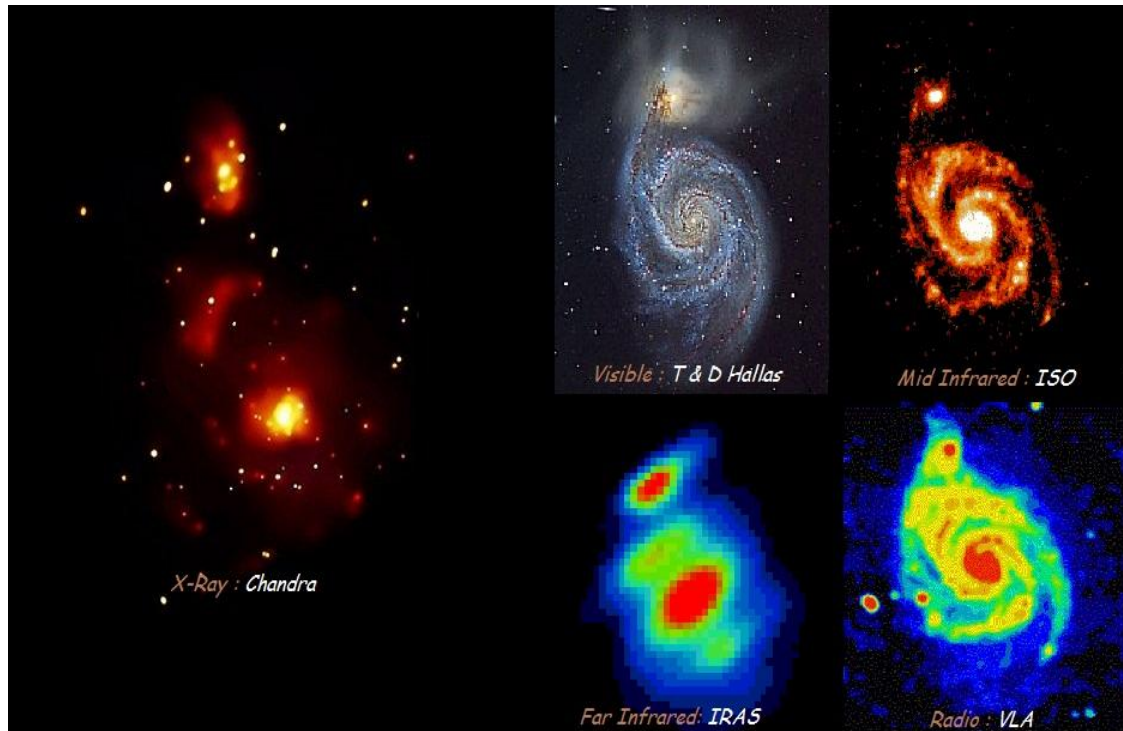


Figure 1.7.—The “Whirlpool Galaxy” (Messier 51), a spiral galaxy that interacts gravitationally with a smaller companion galaxy. In the left there is the X-ray picture obtained with Chandra, in the center up the visible picture obtained with T&D Hallas, in the center down there is the far-infrared picture taken by IRAS, in the right up the mid infrared one taken by ISO and finally down in the right the radio picture taken by VLA (<http://coolcosmos.ipac.caltech.edu>)

1.4.1 Radio Properties

The frequencies corresponding to radio spectrum are those lower than around 300 GHz. The use of radio spectrum in astronomy has many advantages. Firstly, radio waves can penetrate dust, thus with radio telescopes scientists can track hidden objects by dusty clouds and more importantly objects with a great distance from our solar system. Furthermore, with radio telescopes, astronomers can observe ionized Hydrogen something that is making easier to map the Galaxy.

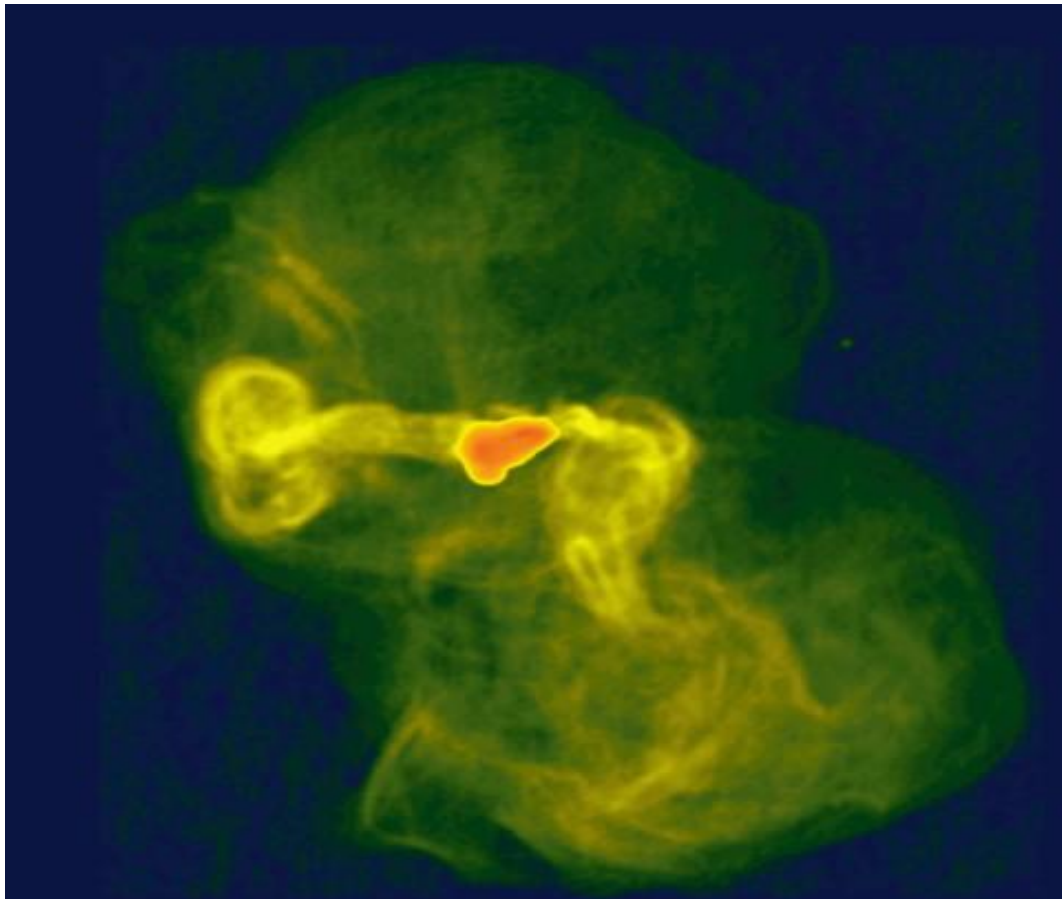


Figure 1.8.—A VLA image of the galaxy M87 radio galaxy. The galaxy's super massive black hole lies within the bright, reddish region. The image was made at a radio wavelength of 900 cm (NRAO/AUI and F.N. Owen, J.A Eilek, N.E Kassim).

The main component of radio emission in AGN is non thermal radiation, more specific, synchrotron radiation. Some AGN reveal strong radio emission in the form of extremely powerful jets that by passing through the host galaxy's interstellar medium diffuse the plasma that exists there and create extended lobes that tend to be edge brightened (Fanarodd&Riley 1974). Generally, AGN radio emission can vary from a few kpcs to more than a Mpc for giant radio galaxies. In Figure 1.8 there is an example of a radio VLA image of a radio galaxy.

1.4.2 Infrared Properties

The infrared radiation, as seen in the *figure 1.6*, lies between the visible and microwave portions of the electromagnetic spectrum. The infrared waves have longer wavelengths than visible and shorter than microwaves. The primary source of infrared radiation is heat or thermal radiation. The sensitivity of infrared detectors is between 1 and 3 microns. Generally infrared radiation is used to observe moderately warm objects. The main advantage in infrared astronomy is the fact that infrared waves penetrate dusty regions of space, allowing us to see areas that emit no light. This means that with infrared telescopes we have the ability to study objects that are hidden by gas or dust, such as the center of our galaxy or a newly forming star. On the other hand, a major problem for infrared astronomy is that the telescope and mirror itself radiated infrared radiation which is making it too hard to observe without the proper systems of cooling the telescope.

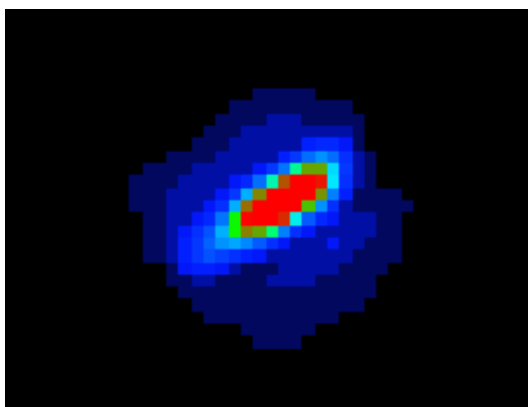


Figure 1.9.- A Mid Infrared image of the starburst galaxy M82 obtained with the IRAS (Infrared Astronomical Satellite) (<http://coolcosmos.ipac.caltech.edu>).

We can divide the infrared spectrum to Near Infrared wavelengths -0.7 to 5 μ m, the Mid Infrared- 5 to 40 μ m, and Far infrared-40 to 350 μ m. There are many attempts since the early 1970's to find active galaxies with ground based observations (Kleinmann &Low 1970; Rieke 1978) that was continued by the start of IR space based observations (de Grijp et al. 1985; Miley et al. 1985; Neugebauer et al. 1986; Sanders et al. 1989). As mentioned above, the advantage of IR AGN observations is the fact that AGN are enclosed in dusty obscure clouds that infrared radiation can penetrate. Thus, AGN are prone to show strong emission at IR wavelengths. There are some photometric techniques that have been developed the past few years for the selection of sources with strong IR emission in the 3-8 μ m range (Lacy et al. 2004; Stern et al. 2005; Polletta et al. 2006; Donley et al. 2007; Fiore et al. 2008). In Figure 1.9 there depicts the starburst galaxy M82 obtained with the IRAS in the Mid infrared part of the electromagnetic spectrum.

1.4.3 Optical Properties

The visible spectrum is the part of the electromagnetic spectrum that responds to wavelengths from 390 to 700 nm or frequency 430-789 THz. The optical spectrum of AGN shows strong emission lines both permitted and forbidden. By the width of an emission line we can collect information for the emitting material. The most identifying feature of an AGN spectrum is the presence of strong emission lines. According to this feature there is another classification for AGN, the AGN *type 1* and *type 2*. In the type 1 category we have objects with a bright continuum and both broad and narrow emission lines, while type 2 AGN we have a weak continuum and only narrow emission lines. At low redshifts type 1 AGN are classified as Type 1 Seyfert galaxies and type 2 AGN as Type 2 Seyferts (Osterbrock 1989). The figure 1.10 is an example of an image in the visible spectrum, obtained by the Australian Astronomical Observatory.



Figure 1.10.- A powerful radio source known as Centaurus A (NGC 5128) Image obtained with AAO.

1.4.4 X-ray Properties

In the electromagnetic spectrum X-rays start at 0.008nm and extend across the electromagnetic spectrum to 10nm. X-ray radiation oscillates at rates between 30×10^{15} hertz and 30×10^{18} . The X-ray emission is expected from astronomical sources which contain extremely hot gas at very high temperatures the range of a million degrees Kelvin to hundreds of millions of degrees. Lower energy X-rays up to 10keV are classified as “*soft*” x-rays, and from about 10 to 120 keV are called “*hard*” x-rays because of their penetrating abilities. X-rays do not penetrate the Earth’s atmosphere, due to that fact they must be observed from above our atmosphere. Generally AGN produce strong absorption features in the X-ray spectra.

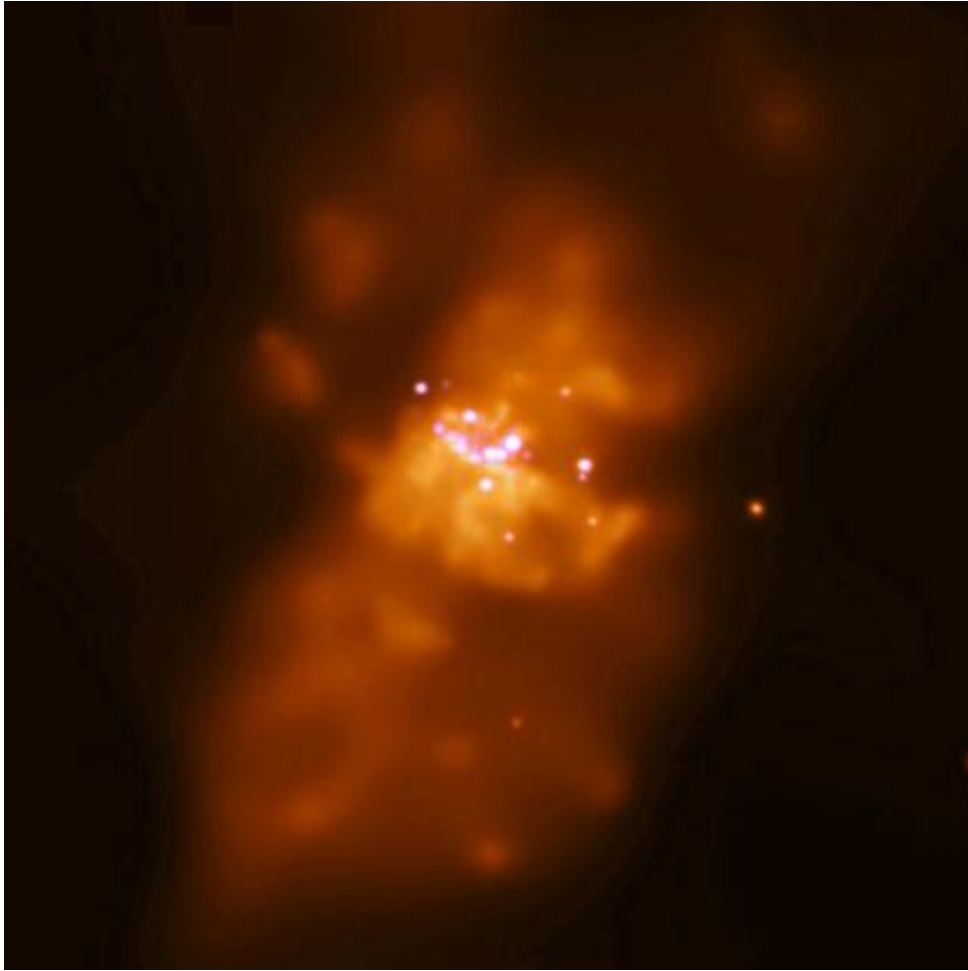


Figure 1.11.- This is M82 a 11 million light years distant starburst galaxy. The bright spots in the middle of the picture are supernova remnants and X-ray binaries whom x-ray luminosity suggests a black hole in the center of the galaxy. This image is obtained by Chandra (<http://chandra.harvard.edu>).

Generally X-ray surveys contribute substantially to our understanding the AGN nature due to the fact that the X-ray background is mostly produced due to accretion onto super-massive black holes. In order to gain new information from an X-ray research in the AGN field we need both “deep” and “wider” X-ray surveys. In this thesis the extragalactic surveys that have been used are the *Chandra* and *XMM-Newton* survey and they are both about to be analyzed in the next chapter.

Chapter 2

Starburst co-evolution

In this chapter I am going to discuss the starburst co-evolution theory and two of the latest models that have been produced to explain it, the merger model by Hopkins (2005) and the semi-analytical model of Croton (2006) for galaxy formation.

2.1 AGN-Starburst Connection, why we believe there is a connection

There are two different ways that very luminous galaxies can be powered-the one is the AGN mechanism, in which the matter forms an accretion disk and falls into the super-massive black hole and the other one is the burst of star formation. A recent conception is that the majority of nucleated galaxies have a super-massive black hole in their center (Rees 1984). Furthermore, there is a significant correlation between the mass of the host galaxy (bulge) M_{bulge} and the mass of super-massive black hole M_{\bullet} :

$$\log\left(\frac{M_{\bullet}}{M_{\odot}}\right) = -1.79 \pm 1.35 + (0.96 \pm 0.12) \log\left(\frac{M_{\text{bulge}}}{M_{\odot}}\right) \text{ (Magorrian et al. 1998)}$$

Where M_{\odot} is the mass of the sun.

According to the Magorrian equation, there is a significant connection between the evolution of the black hole and the evolution of the galaxy itself. Considering the fact that the ratio between the mass of the bulge and the mass of the super-massive black hole is almost constant and similar for active galactic nuclei (AGNs) and normal galactic nuclei (NGNs) (Ferrarese et al. 2001, Gebhardt et al. 2000). Considering the previous fact we come to a very important conclusion that supports the AGN and

starburst connection- The AGN's phenomena aren't connected with the super-massive black hole evolution. Moreover, there is a correlation between the M_{bulge} and the velocity dispersion σ of the host galaxy :

$$\log\left(\frac{M_{\bullet}}{M_{\odot}}\right) = a + \beta \log\left(\frac{\sigma}{\sigma_0}\right) \quad (\text{Tremaine et al. 2002})$$

where β is the slope, σ is the velocity dispersion.

which suggests a joint mechanism by which the bulge and the SMBH are growing together and not the one trigger the evolution of the other. So, after the black hole is established, it cannot be efficiently fueled, thus, the main proof of the coexistence of the AGN and starburst is that there has to be a physical process that links the enormous difference of the bulge and SMBH mass. All that agree to the observed AGN-starburst connection.

2.2 Co-evolution of AGN and Star Formation Rate Density

There are many attempts that have been made in order to construct an explanatory model about black hole and host galaxy evolution. In this co-evolution scenario the evolution of the star-formation rate density has to be related to the number density of bright Quasi-stellar objects (Hopkins & Beacom 2006). The results of this paper is a star formation rate equation that depends on redshift that is based on a review of the uncertainties in the normalization resulting from dust corrections and uncertainties in the employed calibration relations (Figure 2.0).

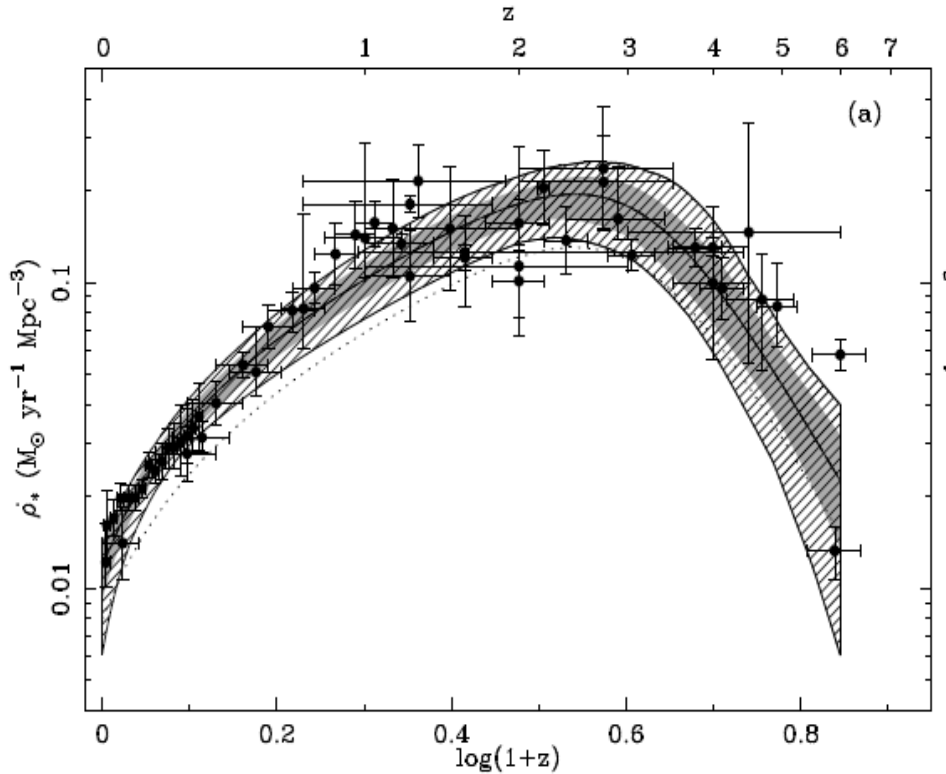


Figure 2.0.— The Star Formation Rate density data used in defining the best fitting parametric forms and the resulting fits (Hopkins & Beacom 2006).

Currently, in Hasinger et al.(2005), there have been catalogued many densities in different luminosity bins of a soft (0.5-2 keV) X-ray sample of 1000 AGNs including *ROSAT*, *Chandra* and *XMM-Newton* surveys. They used two different methods to estimate the AGN X-ray luminosity function and its evolution. The results of the study revealed an early “growth” of the AGN number density at luminosities $L_x \leq 10^{44} - 10^{45} \text{ erg/s}$ and a decline with increasing redshift at $z > 3$. We can conclude to the fact that most galaxies form their stars in the early stages of their lives.

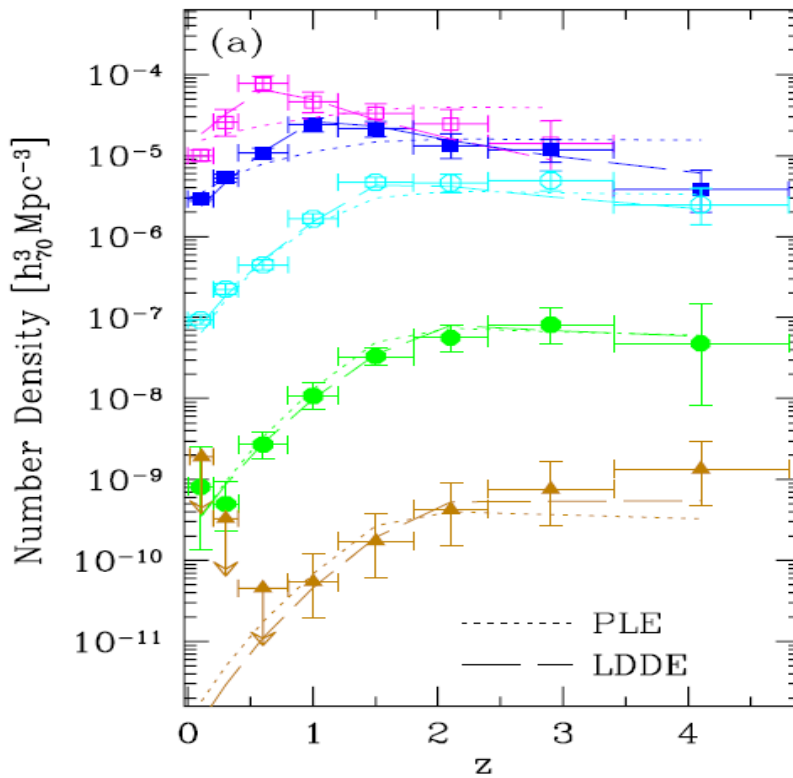


Figure 2.1—The AGN density as a function of redshift in a range of luminosity classes.(Hasinger et al.2005).

2.3 Models to Explain the Co-evolution

Currently, some models have attempted to explain theoretically the above mentioned relation between the host galaxy and the black hole. According to the most prevalent model there is a feedback from accretion of matter onto super-massive black holes, that either disrupts gas cooling in the halo of the galaxy (Croton et al. 2006) or drives gas out of the central galaxy (Hopkins et al. 2006). In this subsection I am going to present these two models.

In Croton et al. 2006 they investigated the role of feedback from radio galaxies and they presented a semi-analytic model for the galaxy formation and evolution and the super-massive black holes, incorporating “radio mode” feedback from AGN, which suppresses gas cooling and thus, it suppresses star formation too in massive host galaxies at higher redshifts. It is called semi-analytic model because in contrast to the full numerical simulations in this model they use approximate prescriptions for physical processes that are poorly understood. They can provide a theoretical framework within which to explore galaxy formation. However, this feedback model that it has been used in Croton et al. 2006 research is rather phenomenological.

The simulation that is being used is the Millennium Run, a very large N-body simulation which follows the hierarchical growth of dark matter structures from redshift $z=127$ to the present, a cut of the Millennium Run simulation for redshift $z=0$ it is presented in Figure 2.2.

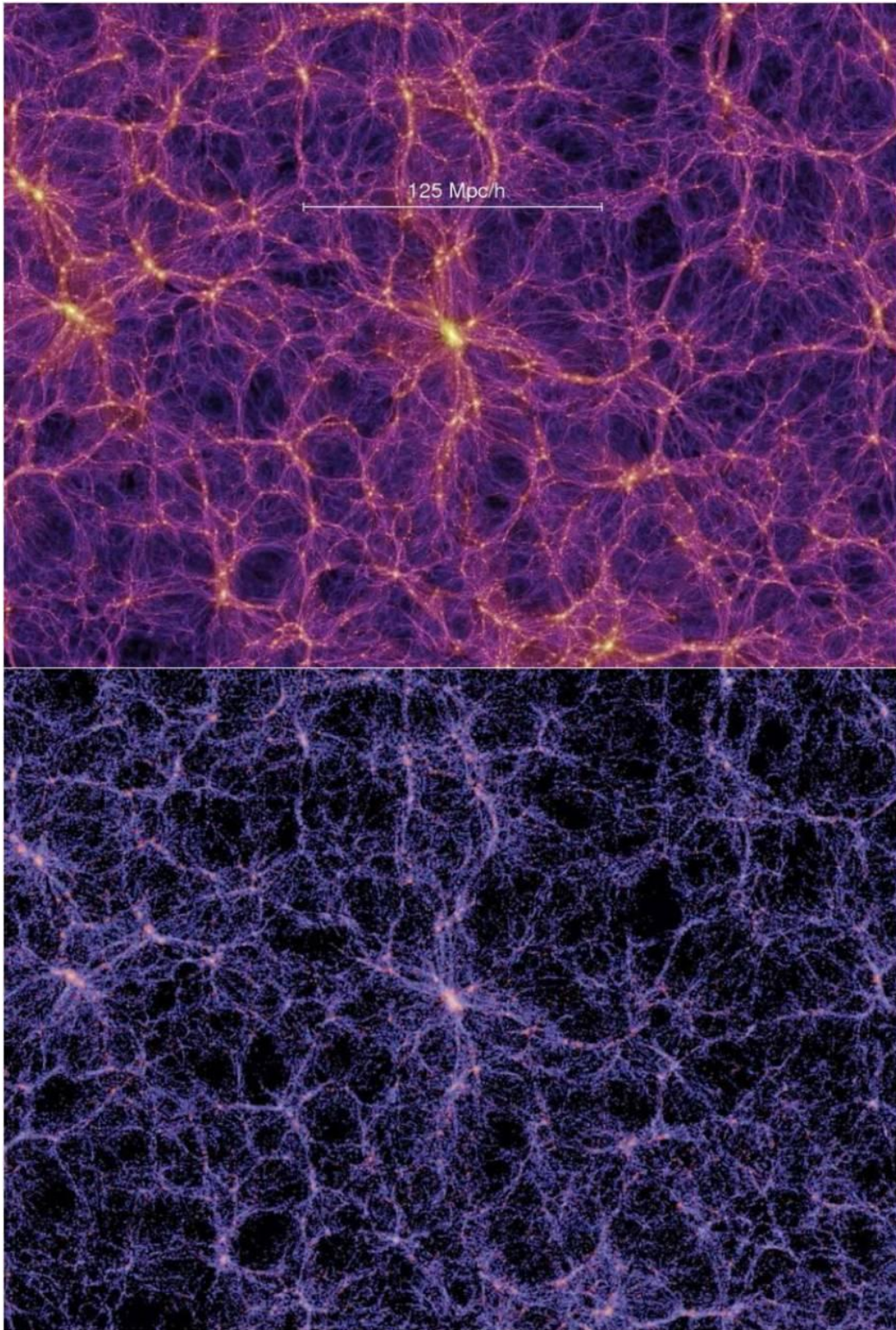


Figure 2.2.—At the top a representation of the distribution of dark matter at zero redshift and at the bottom a representation of galaxy light for a thickness of $15 h^{-1}\text{Mpc}$. This is a result of Croton et al. 2006 by using the Millennium Run. For the figure in the top the color encodes the local velocity dispersion and the intensity the surface density and for the bottom figure intensity encodes the surface brightness and the color the mean B-V color (Croton et al.2006).

The model for star formation in Crotons paper at 2006 is based in the assumption that all star formation occurs in a cold disk gas or in a burst. The gas of the galaxy will be accreted onto the halo along with the dark matter (White & Frenk 1991). Due to the photoionization heating from the UV background the mass of baryonic matter at each point in the halo’s evolution reduces. Thus the gas is shocked to its virial temperature and density as it accretes at the halo virial radius (Shabala & Alexander 2009). Following Croton et al. 2006 the instantaneous SFR is taken to be:

$$\dot{M}_* = a_{SF} \frac{M_{cold} - M_{crit}}{t_{dyn,disk}}$$

Where a_{SF} it the star formation efficiency and it almost equals to 0.1 (Croton et al. 2006), $t_{dyn,disk} = \frac{R_{disk}}{V_{vir}}$ (V_{vir} is the halo virial velocity), M_{crit} is the critical mass.

In *Figure 2.3* we can see the star formation rate density versus the redshift.

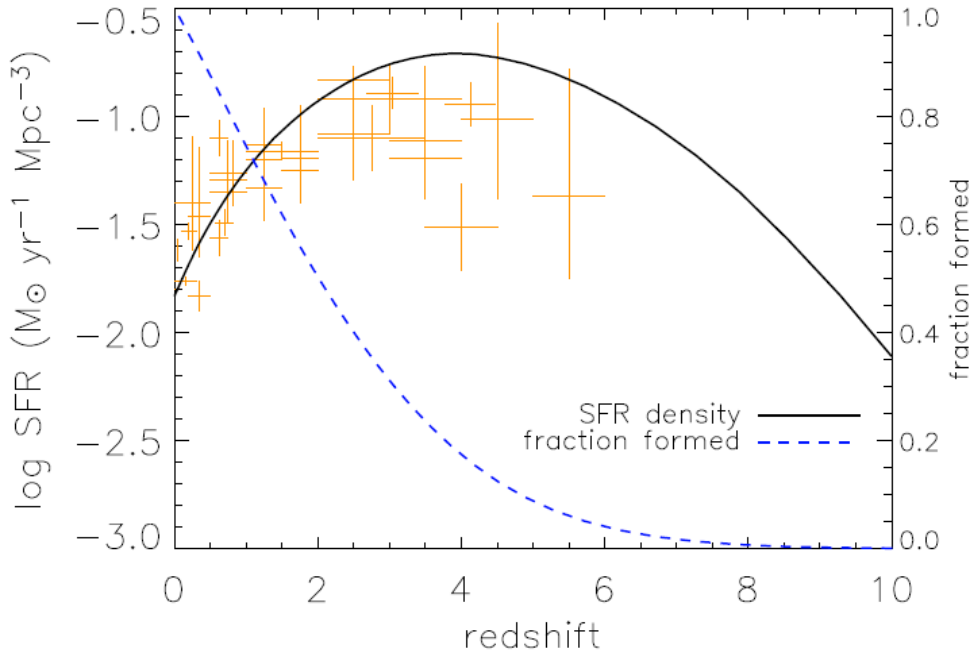


Figure 2.3.—The star formation rate density as a function of redshift. The solid line represents the model that is in agreement with observations. In this model galaxies form a part of their total mass relatively early (Croton et al.2006).

The model that is suggested by Hopkins et al. (2006 e) is based on merger simulations that are performed with the parallel TreeSPH code GADGET-2 (springel 2005). The result is a sub-resolution model through an effective equation of state for star-forming gas (Figure 2.4). The simulation incorporate an energy source in mergers of galaxies that are very abundant in gas which would be able to trigger a bright quasar and show that such an energy injection may have significant impact on the gas of the host galaxy and in that case the result is a production of gas outflows that can affect the central supermassive black hole and lead to its additional growth while suppressing the star formation in the host galaxy. In this model supermassive black holes are represented by “sink” particles that accrete gas at a rate \dot{M} which is estimated from the local gas density and sound speed using an Eddington-limited prescription based on Bondi-Hoyle-Lyttleton accretion theory (Hopkins 2006).

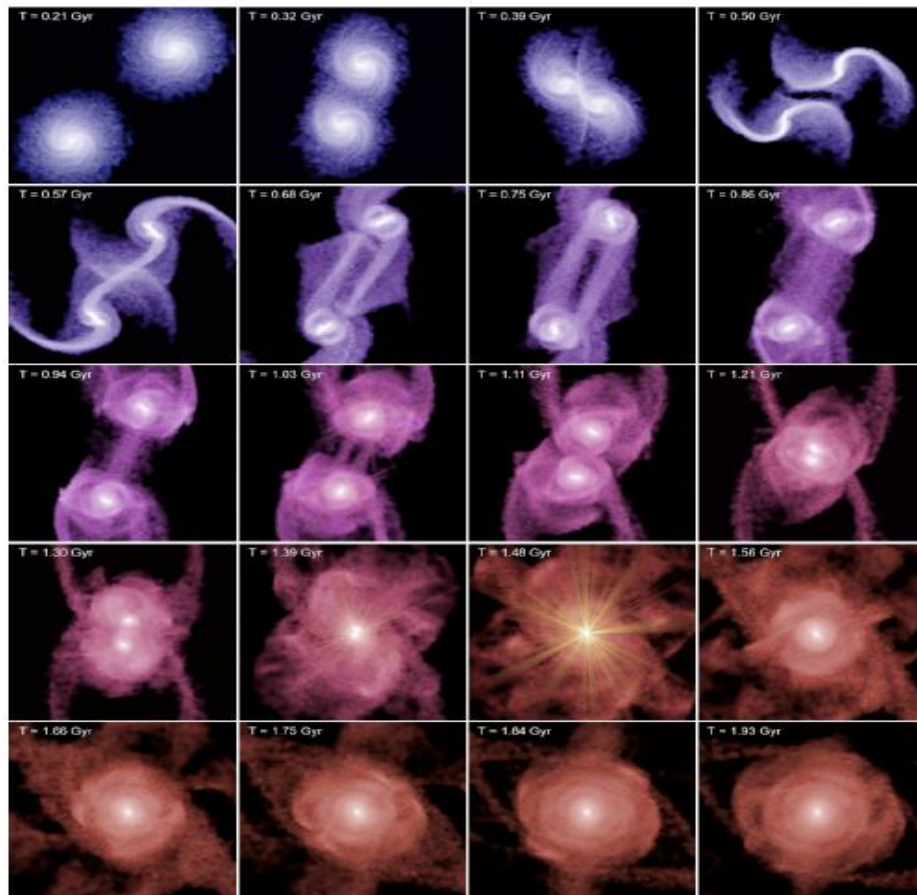


Figure 2.4.— The Hopkins merger model. The gas inflows trigger the supermassive black hole’s accretion and starbursts. The dust and gas clouds make the AGN obscured. Then the AGN feedback sweeps away the gas clouds and as a result it causes star formation and black hole accretion (Hopkins et al.2006)

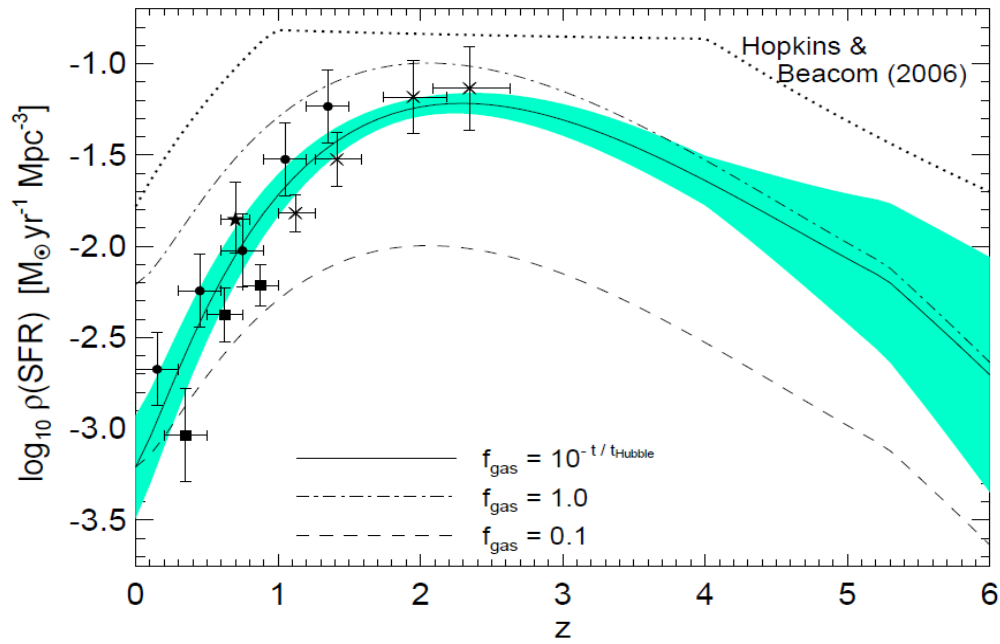


Figure 2.5— The star formation rate density as a function of redshift by the star formation model of Hopkins et al. 2006. The results come from the quasar luminosity function considering an average disk gas fraction :

$$f_{\text{gas}} = 10^{\frac{-t}{t_H}} = e^{-\frac{t}{6\text{Gyr}}}$$

The shaded area represents the 1σ range allowed. The dot-dashed line and dashed lines shows the result that occur assuming that the disk gas fraction is constant with values: $f_{\text{gas}} = 1.0$ and $f_{\text{gas}} = 0.1$. The dotted lines represent the result from Hopkins & Beacom (2006) observations.

2.4 Support of the Merger Model

The age of galaxies can be estimated by their colors. Thus, we can divide them in blue and red galaxies. The younger ones give a color closer to blue which reveals that they have high rates of star formation. In the other hand, older and evolved galaxies that have stopped their star forming process emit light in the red light spectrum.

In Willmer et al. 2006 a sample of more than 11,000 galaxies from the DEEP2 Redshift Survey was divided into predominantly red and blue galaxies. The luminosity function of each color type galaxy evolves with a different way (Figure 1.6a). Blue galaxies don't show a significant change in overall number density, yet they have a large amount of luminosity evolution, generally they are shifted to brighter magnitude at constant number density whereas red galaxies' luminosity remain almost constant but they present a larger change in number density. The sample that is used in Willmer et al. 2006 can be used to support the model that merger-driven feedback from an AGN may quench star formation while contributing to the order of magnitude decline in the star formation rate(Figure 2.6b).

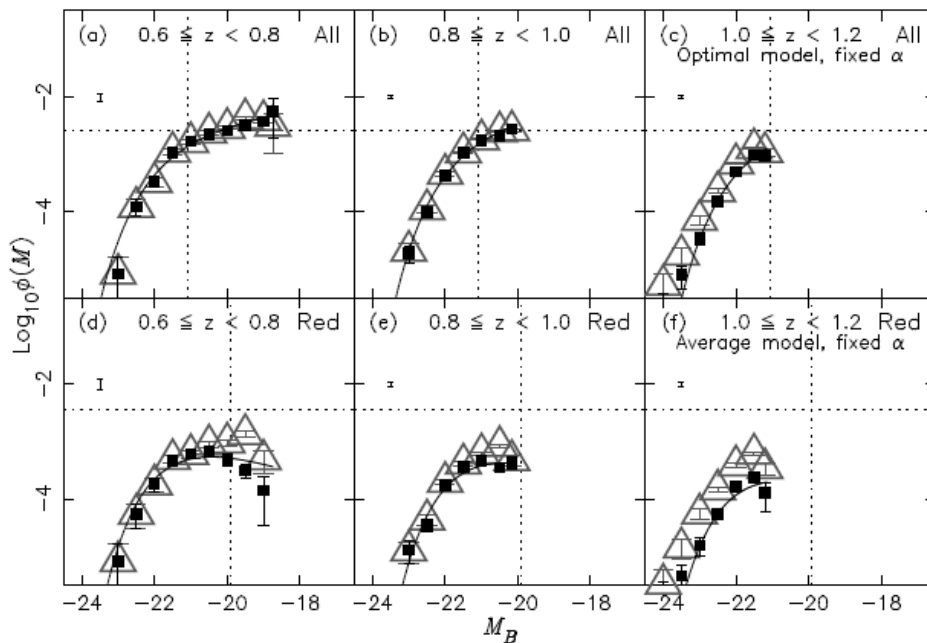


Figure 2.6a—Luminosity function for both DEEP2 All and Red galaxy samples versus magnitude. The triangles are strict upper limits to the galaxies' density under the assumption that all failed-redshift red galaxies are located only in that bin. (Willmer et al.2006).

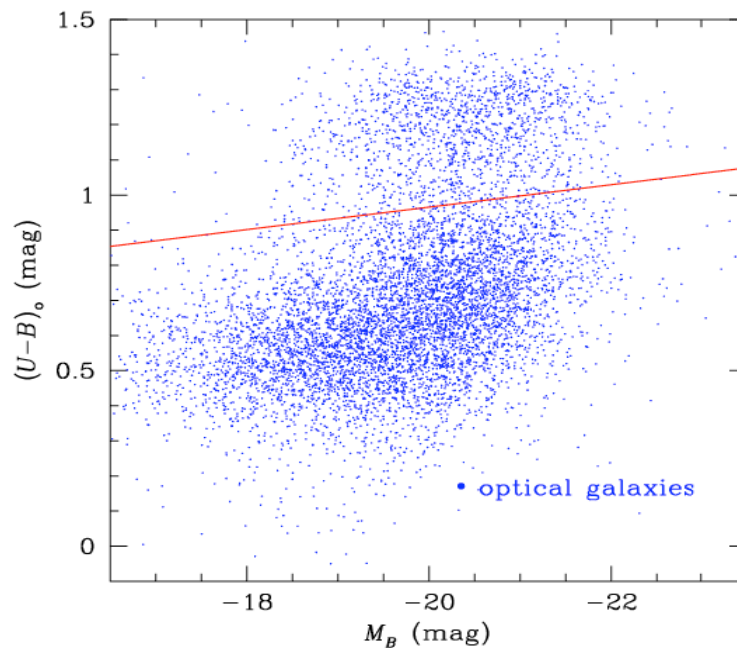


Figure 2.6b.—Rest-frame color- magnitude diagram for DEEP2 for redshifts $0.4 < z < 1.4$. The dotted line denotes the cut used to define red-sequence galaxies and is the same at all redshifts (Willmer et al.2006).

2.5 Problems with the Merger Model

Recently published works present some contradictions to the merger model. In Nandra et al. 2007 in order to comprehend the relation between rest-frame color and optical luminosity, there has been a selection of 68 AGN x-ray sources from *Chandra* survey in the range of $0.6 < z < 1.4$. After analyzing and matching the sources with other catalogues they came to the conclusion that the great majority of the 68 AGN sample lie on the red sequence, at the top edge of the blue cloud, and the region in between (Figure 2.7).

The Hopkins model predicts that due to the fact that star formation is quenched before the red sequence migration, an AGN should be obscure because of the star formation and have hard x-ray spectrum and when it reach the state of migration it should blow it's star forming gas out of the galaxy, thus, stop being obscured and have a soft x-ray spectrum. The fact that there is a great number AGNs in the red sequence at $z \approx 1$ shows that AGN don't stop being active after the quenched of star formation. Furthermore there have been observed many soft X-ray sources among the blue galaxies and on the other hand many hard X-ray sources on the red sequence which contradicts to Hopkins scenario.

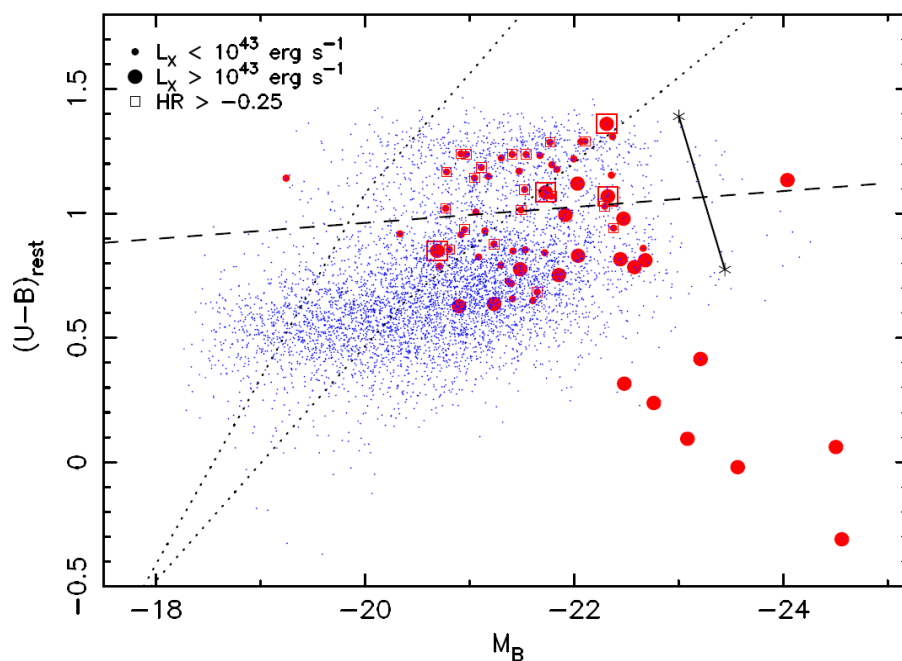


Figure 2.7.—Rest frame $U-B$ color against B -band absolute magnitude. The Blue dots represent the DEEP2 galaxies and the red dots the X-ray sources, Squares indicate hard X-ray sources, larger dots indicate more luminous systems. The dashed line shows the limits between red and blue galaxies (Nandra et al.2007)

Another research that is in contrast to the merger model is presented in Schawinski et al.2009. They examined a sample of both unobscured and obscured AGN by using the hard x-ray selection. As a result they detected a very small number of AGNs in the peak of the blue cloud. The migration from the blue cloud to the red sequence lasts approximately 1 Gyr and the peak of star formation occurs with a delay of 100 Myrs from the detectable black hole growth. There are presented two possible scenarios that can justify these facts. The first one suggests that AGNs do suppress star formation but due to the large difference between the typical lifetime of an AGN and the time of suppression most AGNs have migrate from the blue cloud. Another scenario suggests that star formation is suppressed immediately but we observe the AGN luminosity after 100 Myr (Schawinski et all 2009a). In Hopkins et all 2006 the merger model that is described predicts a coeval maximum black hole growth and a peak of star formation. If that would apply there should be a large number of AGNs in the blue cloud.

Chapter 3

Sample Selection

The selection of multiwavelength surveys is the most efficient choice to study AGNs. Due to the fact that AGNs in different wavelength have diversity in their appearance, a survey at an only one particular wavelength doesn't guarantee realistic results. Even if Hard X-rays (2-10 keV) can penetrate obscuring dust and gas columns there is a chance that AGN with high absorbing columns will be missed. So if X-ray surveys would be combined with infrared and radio observations the AGNs that have been missed would probably be identified (Donley et al. 2005a,b). Furthermore, According to the deepest *Chandra* and *XMM* observations the vast majority of the X-ray sources that are observed should be AGN (Barger et al. 2003).

For the study of AGN we have selected data from several different catalogs of both space and ground based observatories (that are described above) and cover two regions of the sky, ELAIS N1 and the Lockman hole (Figure 3.2). In this section, I am going to describe the space and ground observatories with the parent catalogs that we have used for this research and then the final sample and its properties in the different parts of the electromagnetic spectrum.

3.1 The Spitzer Space Telescope (SST)

The Space Infrared Telescope (SST) (<http://www.spitzer.caltech.edu>) is an infrared space observatory that was launched into space in 25 August 2003 by NASA (Figure 3.1). Initially Spitzer was launched on a two and a half year mission. With a 0.85m mirror, it was the largest infrared telescope ever launched into space and it brought to scientist very important information and a world that they had never seen before. In order to reduce the amount of coolant that it would needed, Spitzer was placed to follow an heliocentric orbit unlike the majority of the satellites that have been launched into space .

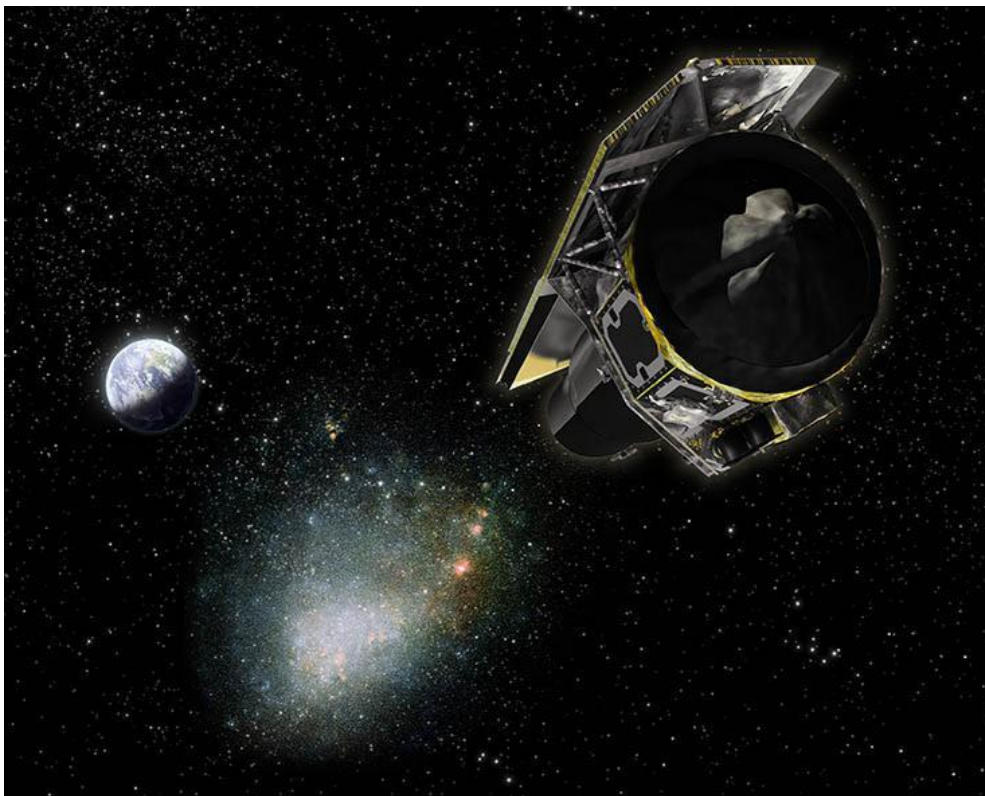


Figure 3.1 .—An artist's conception about Spitzer space telescope (Nasa).

The observational wavelength of the Spitzer telescope is 3-180 μm . The satellite contains three instruments.

- An infrared array camera (IRAC) that covers bands centered at 3.6, 4.5, 5.8, and 8.0 μm .
- An infrared spectrograph (IRS) which is a low and moderate resolution spectrograph spanning 5.2 to 38 μm , and

- A Multiband Imaging Photometer (MIPS) that is covering bands centered nominally at 24, 70 and 160 μm .

3.1.1 SWIRE Redshift Catalog

SWIRE or else the Spitzer Wide-area Infrared Extragalactic Survey is the largest Spitzer legacy program and it covers 49 square degrees among six different directions on the sky in all seven Spitzer bands (3.6 μm , 4.5 μm , 5.8 μm , 8 μm , 24 μm , 70 μm and 160 μm), selected from the entire IRAS/DIRBE sky as the areas with the lowest 100 μm surface brightness. Swire is a medium depth survey that can trace AGN, the evolution of dusty and star forming galaxies and evolved stellar populations. It can detect a typical galaxy to a redshift of $z \geq 2.5$ which gives us a distance of over 10 billion light years away. Until now 1025119 redshifts are documented (Robinson M. et al. 2008)

The SWIRE goal is to study and record the evolution of active galactic nuclei, starbusts, spheroidal galaxies. The observed areas were selected such that the sample would include many different environments. The main purpose of the survey is to detect galaxies far enough that will provide us the coveted information of how the Universe looked when it had its present half age. The Swire survey has fructify with outcomes as the discovery of 2.3 million galaxies at 3.6 μm and almost 350000 at 24 μm .

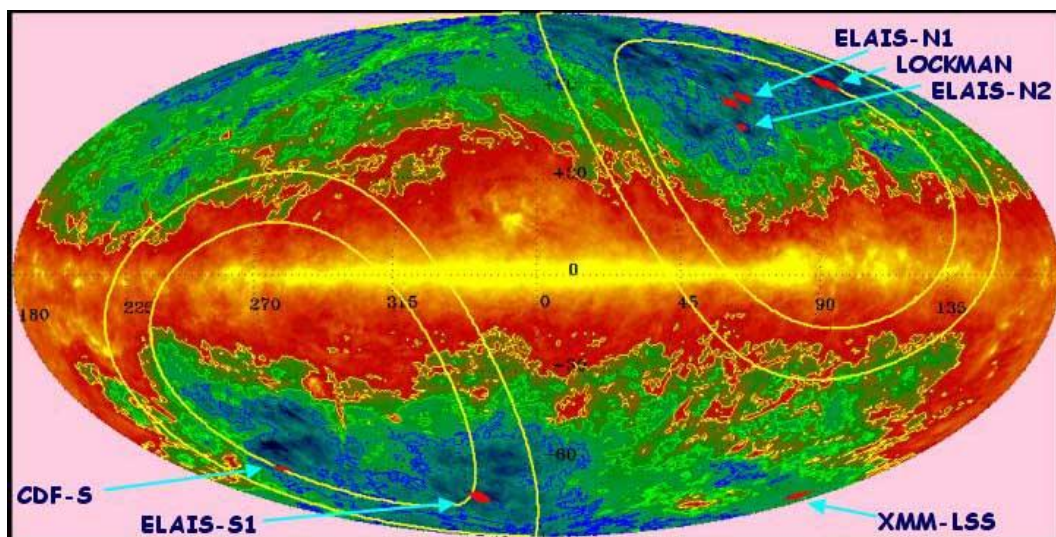


Figure 3.2.— The SWIRE Survey Fields are shown in red. The contour levels in blue, green yellow are respectively 1, 2, 4 MJy/sr.

Chapter 3 – Sample Selection

The SWIRE data include IRAC (Infrared Array Camera) 3.6, 4.5, 5.8 and 8.0 μm and MIPS (Multiband Imaging Photometer): 24, 70 and 160 μm . Also it include optical Ancillary for selected regions. This optical data in most cases is u, g, r, i, z and bands from the 2.5 m Isaac Newton Telescope in La PALMA that was taken in conjunction with the ELAIS survey or from new data originating primarily at KPNO and CTIO.

The data that are released include data from all 6 regions on the sky, known as ELAIS-N1, ELAIS-N2, XMM-LSS, The Lockman Hole (LH), ELAIS-S1 and Chandra Deep Field South (CDFS) (Figure 2.0). More information about the Swire survey areas and the observation are mentioned in the Table 2.1. The imaging products of the SWIRE survey consist of several different parts:

- Coadded mosaic images, one per each IRAC bands of 3.6, 4.5, 5.8, and 8 μm . These data are tiled.
- Three coadded mosaic images, one for each of the MIPS bands of 24, 70, and 160 μm which is supplied as one image for the entire field.
- Optical Images in the five optical bands: u, g, r, i, z. These data are also tiled.
- Some smaller mosaic images that are used for understanding the data coverage
- Pseudo-true color images made from the IRAC bands.

	RA	Dec	ISSA MJy/sr	E(B-V)	Size Sq. deg
ELAIS-S1	00 ^h 35 ^m 00 ^s	-43° 40'	0.42	0.008	7.0
XMM-LSS	02 ^h 21 ^m 20 ^s	-04° 30'	1.3	0.027	9.2
Chandra-S	03 ^h 32 ^m 00 ^s	-28° 16'	0.46	0.001	8.0
Lockman	10 ^h 47 ^m 00 ^s	+58° 02'	0.38	0.006	11.0
ELAIS-N1	16 ^h 11 ^m 00 ^s	+55° 00'	0.44	0.007	9.2
ELAIS-N2	16 ^h 36 ^m 48 ^s	+41° 02'	0.42	0.007	4.8

Table 3.1.— The first column is the field name, the second is right ascension, next is the Declination of the field center, the forth is the infrared background emission at 100 μm band fifth is the color excess E(B-V) and the last one is the size in square degrees.

3.1.2 SWIRE ELAIS-N1 Infrared

This sample consists of 35 AGN with spectroscopic redshifts selected from the Spitzer Wide-Area Infrared Extragalactic Survey (Lonsdale et al.2003&2004). The sample is being observed in the 3.6, 4.5, 5.8 and 8 μm bands with the IRAC and in the 24, 70 and 160 μm bands with the Multiband MIPS.

3.1.3 SWIRE ELAIS-N1 optical

For the optical catalog the MIR band catalog in SWIRE ELAIS N1 was associated with the INT (Isaac Newton Telescope) optical five-band (u, g, r, I, z) catalog. The area of the INT CCD survey is approximately 100 deg^2 thus it covers only 7 deg^2 of the SWIRE EN1 field. The camera consists of close packed mosaic of 4 thinned EEV42 2kx4k CCDs. The CCDs have a pixel size of 13.5 microns corresponding to 0.33 "/pixel.

The resulting catalog of INT and SWIRE merging consists of approximately 293,000 objects.

3.2 Chandra Space Telescope

Chandra X-ray observatory (<http://chandra.harvard.edu>) is a satellite launched on 23th of July, 1999 (Figure 3.3). Chandra is an x-ray telescope much more sensitive than any previous X-ray telescope (observes 100 times fainter sources). Chandra instruments are the followings:

- An advanced CCD imaging spectrometer that consists of 10 CCD chips and provides images and spectral information of the observed object. It operates in the range of 0.2-10 keV.
- A High Resolution Camera which has the ability to move into position during an observation. It consists of two micro-channel plate components and images over the range of 0.1-10 keV.



Figure 3.3.—An artists conception of Chandra Space Telescope (Nasa).

- A High Energy Transmission Grating Spectrometer that works over the range of 0.4 – 10 keV and has a spectral resolution of 60-1000.
- A Low Energy Transmission Grating Spectrometer that has a tange of 0.09-3keV and a resolution of 40-2000.
- A High Resolution Camera which has the ability to move into position during an observation. It consists of two micro-channel plate components and images over the range of 0.1-10 keV.

Chandra follows an elliptical orbit of altitude 133,000 km and its closest approach to Earth is 16.000km. A complete orbit takes approximately 64 hours and 18 minutes (Figure 3.4)

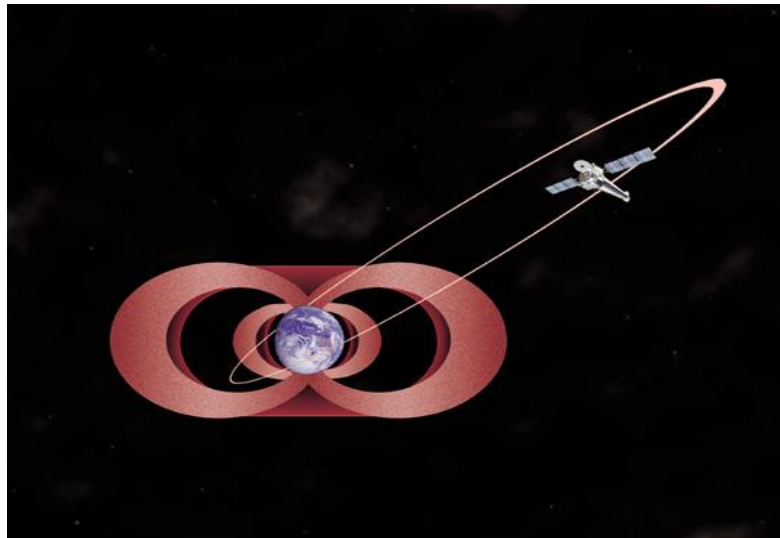


Figure 3.4 .— Illustration of Chandra's elliptical orbit (<http://chandra.harvard.edu>)

3.2.1 Chandra ELAIS-N1 survey

This catalog, (Georgakakis et al. 2008), contains a sample of 6295 unique sources over an area of $11,8 \text{ deg}^2$.

With a new technique that has been used, it is estimated the X-ray source counts in 4 different energy bands: soft (0.5-2 keV), hard (0.5-10 keV), ultra-hard (2-10 keV) and total (5-10 keV), by combining deep pencil-beam and shallow wide-area. The catalog comes from 6 different Chandra surveys (Table 1), both deep pencil-beam and shallow wide -area.

The first survey is the Chandra Deep field North and South survey (CDF-N/S), the second one is the Extended Chandra Deep Field South (ECDFS), the Extended Groth Strip (EGS) is another one, the ELAIS-N1 (EN1) and finally the XBOOTES survey. The data from these surveys are analyzed in similar methods to those that are described by Nandra et al.2007; Laird et al.2009.

Survey	Obs. IDs	Exposure (ks)	Area (deg ²)	Sources
(1)	(2)	(3)	(4)	(5)
CDF-N	580, 957, 966, 967, 1671, 2232, 2233, 2234, 2344, 2386, 2421, 2423, 3293, 3294, 3388-3391, 3408, 3409	2000	0.11	516
CDF-S	581 441 582 1672 2405 2239 2312 2313 2406 2409 1431	900	0.06	270
ECDF-S	5015-5022, 6164	250	0.25	592
EGS	3305, 4357, 4365, 5841-5854, 6210-6223, 6366, 6391, 7169 7180, 7181, 7187, 7188, 7236, 7237, 7238, 7239	200	0.63	1325
EN1	5855-5884	5	1.47	545
XBOOTES	3596-3660, 4218-4272, 4277-4282	5	9.24	3056

Table 3.2.— The first column of table 1 describes the name of the Chandra Survey. The second records the observation IDs that have been used. The next is the exposure time in ks. The forth column describes the total surveyed area in deg², and the last column gives the total number of sources in each

3.2.2 The SWIRE/Chandra Survey: The X-ray Sources

The SWIRE/Chandra catalog (Wilkes et al.2009) contains 775 X-ray sources that were detected in a moderate-depth (70ksec) Chandra survey, in the Lockman hole Field of the Spitzer/SWIRE Legacy survey coincident with an ultra-deep VLA survey. The 99% (771) of the X-ray sources have infrared or optical counterparts and 333 of them have MIPS 24 μ m detections.

3.3 Giant Metrewave Radio Telescope

GMRT is the world's largest array of radio telescopes at meter wavelengths. It is located at a site 80 km north of Pune, India. It consists of 30 fully steerable gigantic parabolic dishes, 45m diameter each, that are spread over distance of 25 km. Due to the number of the dishes astronomers can achieve a higher sensitivity at high angular resolution as well as the ability to image the radio emission from diffuse extended regions. Fourteen of the dishes have a random location in a compact central array in a region of about 1km^2 . The rest of them are forming 3 arms in an approximately Y-shaped configuration over a much larger region with the longest arm to spread in 25km.

The array operates in six frequency bands centered at: 50, 153, 233, 325, 610, and 1420MHz. The highest angular resolution that GMRT can achieve has a range from about 60 arcsec at the lowest frequencies to 2 arcsec at 1.5GHz.



Figure 3.5.—A picture of GMRT taken in January 2001.

3.3.1 325-MHz Observations of the ELAIS-N1 field

In this catalog (S. K. Sirothia et al. 2008) they were detected 1286 sources at 325 MHz with a total flux density above $270\mu\text{Jy}$, and towards the center of the field ($16^{\text{h}}10^{\text{m}}, +54^{\circ}36'$), using the Giant Metrewave Radio Telescope (GMRT). The data of this catalog are combined from two different days with an rms noise of 40 mJy beam^{-1} . The ELAIS-N1 field has been selected in a sky region that has low IR foreground emission, to allow detection of fainter, thus more distant galaxies. More details about the observation are given in table 2.

Date	2005 June 26, 2005 June 27
Working antennas	25
Centre Frequency	325 MHz
Bandwidth	32 MHz
Visibility integration time	4.19 s
Total observation time	10.3 hrs \times 2

Table 3.3.—The observation summary of S. K. Sirothia et al. 2008.

3.3.2 610-MHz Observations of the ELAIS-N1 field

In this catalog (Garn et al. 2007), the region in the sky “ELAIS_N1” was observed for 25 hours. The observations were spread to three days in August 2003, using the GMRT operating at 610 MHz. The observation were centered at $16^{\text{h}}11^{\text{m}}00^{\text{s}}$, $55^{\circ}00'00''$. There were observed nineteen pointings that were spaced by 36' in a hexagonal grid in order to get nearly uniform coverage of the region. The nineteen points are covering a total area of approximately 9 deg^2 with a resolution of $6 \times 5 \text{ arcsec}^2$.

Four of the total number of pointings that were observed, were deep observations with an rms of almost $40 \mu\text{Jy}$ while the rest of them had an rms of approximately $70 \mu\text{Jy}$. After some techniques used for data reduction and production of a mosaic image of the region, a catalog of 2500 detected sources at 6σ was presented.

3.4 Very Large Array - VLA

The Very Large Array, or VLA (<http://www.vla.nrao.edu/>) is a radio astronomy observatory which is located on the Plains of San Agustin, 80 km west of Socorro, New Mexico (Figure 3.6). The VLA consists of 27 telescopes that are built at an elevation of 2124 above the sea level, each of them has a dish diameter of 25 meters and a height of 209 metric tons. The antennas are arrayed along the three arms of a Y-shape as it is demonstrated in the picture, and by using railroad tracks can be relocated to a number of prepared positions which allow them aperture synthesis interferometry with a maximum baseline of 36km.

The frequency that VLA covers varies from 74 to 50,000 MHz (a wavelength from 400 to 0.7 cm). The smallest angular resolution that can be reached is about 0.05 arcseconds at a wavelength of 7mm. VLA's angular resolution range from 0.05 to 700 arcsec. The VLA has made key observations of black holes and protoplanetary disks around young stars and has provided a large amount of new knowledge about the physical mechanisms that produce radio emission.

Nowadays, the VLA is being transformed into a new research instrument. This transformation will be complete by 2012 when it will be presented the Expanded Very Large Array or EVLA, which will be 10 time more sensitive than the VLA, and will give scientist the chance to explore the universe furthermore.



Figure 3.6.— In the left a picture of VLA as seen from the north, in the right a close-up picture of one of VLA's dishes (<http://www.vla.nrao.edu/>).

3.4.1 VLA First Survey

FIRST- Faint Images of the Radio Sky at Twenty-one Centimeters- VLA Survey (Becker, White & Helfand 1995) began in spring 1993 and it covered over 9,900 square degrees of the North Galactic Cap at 1.4 GHz.

The First Survey Catalog include peak and integrated flux densities and size information derived from fitting two dimensional Gaussians to the sources that are generated from the coadded images. The catalog contains 816,331 sources that derive from 1993 through 2004 observations. Approximately 15% of the sources have optical counterparts at the limit of the POSS I plates where $E=20.0$. In the following Figures 3.7 & 3.8, it is presented the coverage of the northern and southern sky separately.

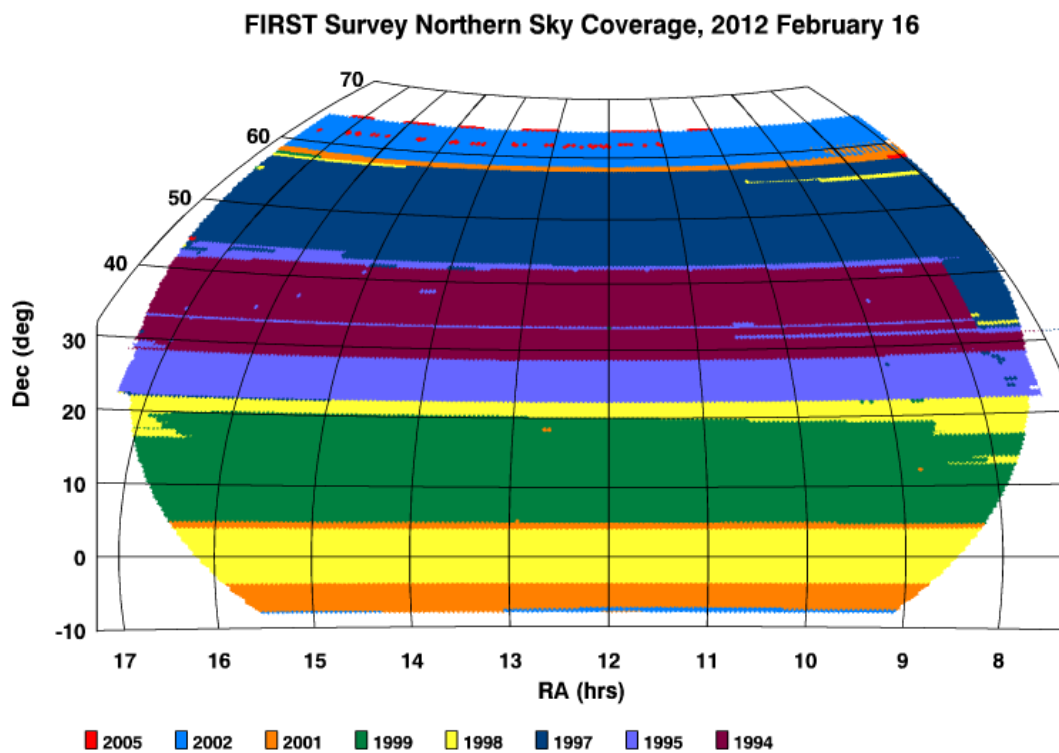


Figure 3.7.- The northern sky coverage of the survey. The different colors represent the different years that survey had been held.

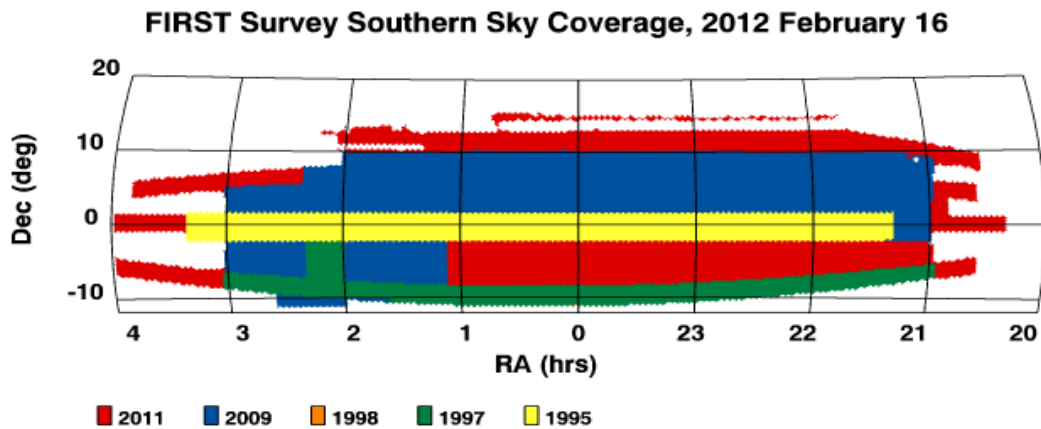


Figure 3.8.- The southern sky coverage of the survey. The different colors represent the different years that survey had been held.

3.4.2 Deep VLA Survey at 20 cm

This 20cm radio survey (P. Ciliegi et al. 1998) covers the region of the sky ELAIS-N1. Its flux limit varies over area survey from a 5σ limit of 0.135 mJy over an area of 0.12 deg^2 to 1.15 mJy. This catalog contains a total number of 867 radio sources, 428 of which form a complete sample in a flux range of 0.2-1.0 mJy. The catalog reports the name of the sources, the peak flux density S_p , the total flux density in the radio RA and DEC, the FWHM of the major and minor axis in arcsec, the positional angle of the major axis in degrees and the off-axis value in the VLA map in arcmin.

3.5 XMM-Newton

The XMM-Newton observatory (X-ray Multi –Mirror Mission-Newton) was launched by ESA in December 1999. It is placed in a 48 hour elliptical orbit at 40° with its apogee and perigee being approximately 114,000 and 7,000 km from Earth. XMM-Newton satellite consists of three X-ray telescopes with an unprecedented effective area that are sensitive over the energy range of 0.2 keV to 12 keV. The combined collective area is $4,300 \text{ cm}^2$ which provides highly sensitive observations. Furthermore it holds two reflection grating spectrometers which are sensitive below 2keV, and an additional optical/UV telescope of 30 centimeters diameter.



Figure 3.9.— An artists conception for XMM newton satellite. (<http://xmm.esac.esa.int/>).

3.5.1 XMM-Newton catalog of the Lockman Hole

The XMM-Newton catalog (Brunner et al. 2007) is an X-ray catalog in the sky area of Lockman Hole of Lowest Galactic line-of-sight column density $N-5.7 \cdot 10^{19} \text{ cm}^{-2}$. It was observed by the XMM-Newton X-ray observatory in 18 pointings for 1.16Msec. The exposure was 637 ks. The analysis which was performed was a result of the XMM-SAS data analysis package version 6.0 (Brunner et al.2007).Twelve of the pointings found were centered at $+10^{\text{h}}52^{\text{m}}43^{\text{s}}$, $57^{\circ}28'48''$ (j2000) with some offsets of $15''$, while the remaining ones were spread over about $30'$ in right ascension.

3.6 *The Final Sample and Properties*

The final catalog consists of 501 sources observed in two different areas of the sky, the ELAIS N1 and the Lockman Hole (Figure 2.0). The x-ray luminosities L_x of the sample's sources vary from about $10^{40} < L_x < 10^{46}$ erg/s. If a quasar is identified as a luminous X-ray source with $L_x > 10^{42}$ erg/s we can state that it contains a luminous AGN in its core (Brandt & Hasinger 2005; Barger 2003). This luminous X-ray emission could be associated to either AGN activity with extinguished optical spectroscopic signatures (Moran et al. 2002; Maiolino et al. 2003; Goulding & Alexander 2009), or to star formation activity (Jackson et al. 2012). The sources with hard x-ray luminosity from about $L_x = 10^{42-44}$ erg/s are characterized as AGNs (Alonso-Herrero et al. 2006; Almeida et al. 2008) although they could be AGNs that have strong X-ray emission due to that fact that very few starburst galaxies have been observed with $L_x > 10^{42}$ erg/s, even including luminous sources at moderate redshifts (Zezas et al. 2001). The sources with lower luminosities than the limit above are considered to be normal galaxies with high rated of star formation. In the following diagram I present the X-ray luminosity versus the redshift of the 501 sources of the final catalog. For the calculation of the sources' redshifts we used the usual flux-luminosity relation with the following values for the cosmological constants: $\Omega_\Lambda = 0.7$, $H_0 = 72.6$ km/sec/Mpc, $\Omega_M = 0.3$. As a result we found 17 sources with $L_x < 10^{42}$ erg/s that can be categorized in the normal starburst galaxy class (non AGN), 151 sources that have $10^{42} \leq L_x \leq 10^{44}$ erg/s and are AGN sources that are dominated from star forming regions and 184 sources that are QSOs, AGNs that don't have a high star forming rate. Those results are not surprising because our sample is selected in the x-ray spectrum, thus it is expected the majority of our sources to have an active galactic nuclei in their center.

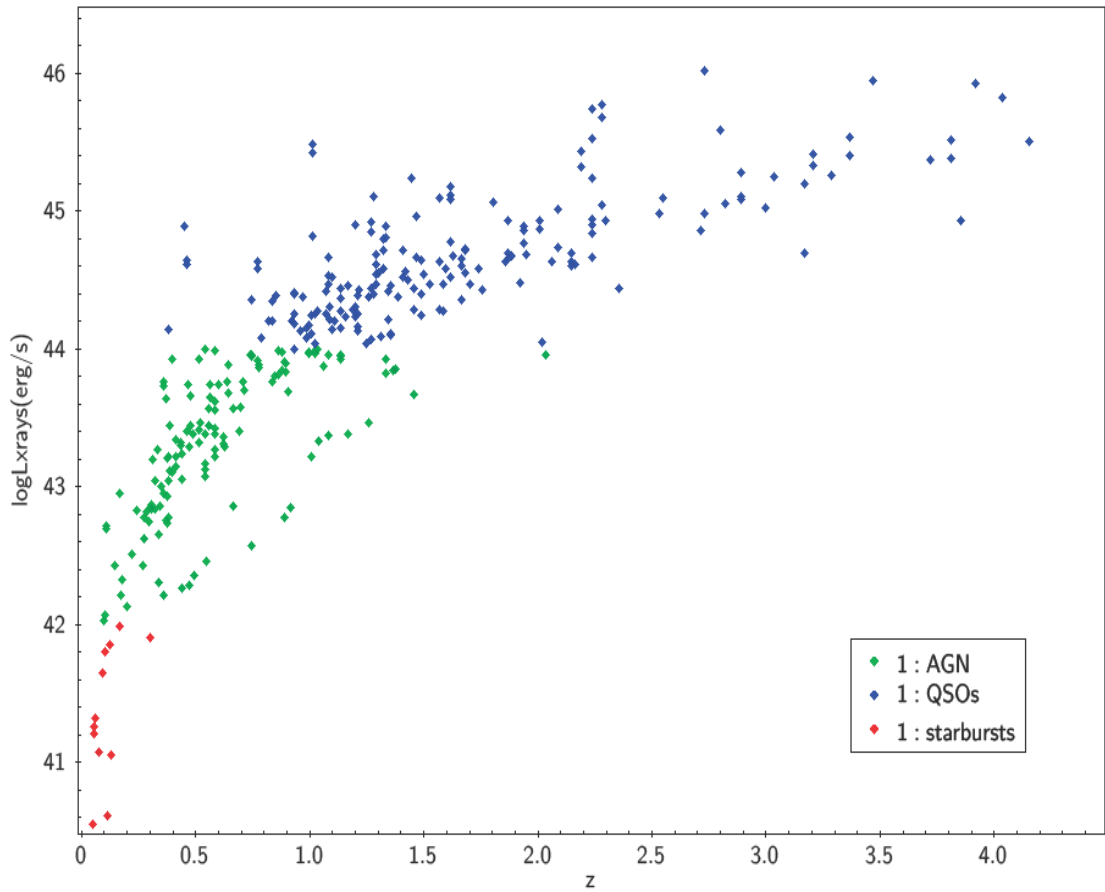


Figure 3.10.- hard X-ray luminosity in erg/sec versus redshift. The sources have been divided in 3 categories the normal starbursts (non AGN) with $L_x < 10^{42}$ erg/s are presented with a grey color, the starburst dominated AGN galaxies with $10^{42} < L_x < 10^{44}$ erg/s with a green color and QSO's with $L_x > 10^{44}$ erg/s and a blue color.

The results in figure 3.10 are quite biased because of our limited observational abilities for objects that are very distant to us. Normally we should observe sources with lower luminosities too in redshifts higher than Figure 3.10 but generally sources with big distances thus a big redshift have to have a very high luminosity in order to be observed from our telescopes.

In our sample the radio luminosity vary between the values of:

$$10^{20} < L_{radio} < 10^{27} W$$

From our 501 sample 99 of our sources have radio counterparts. 48 of our sources as seen in figure 3.11 have $L_{radio} > 10^{24}$ w which makes them powerful radio sources and most likely to host an AGN in their center.

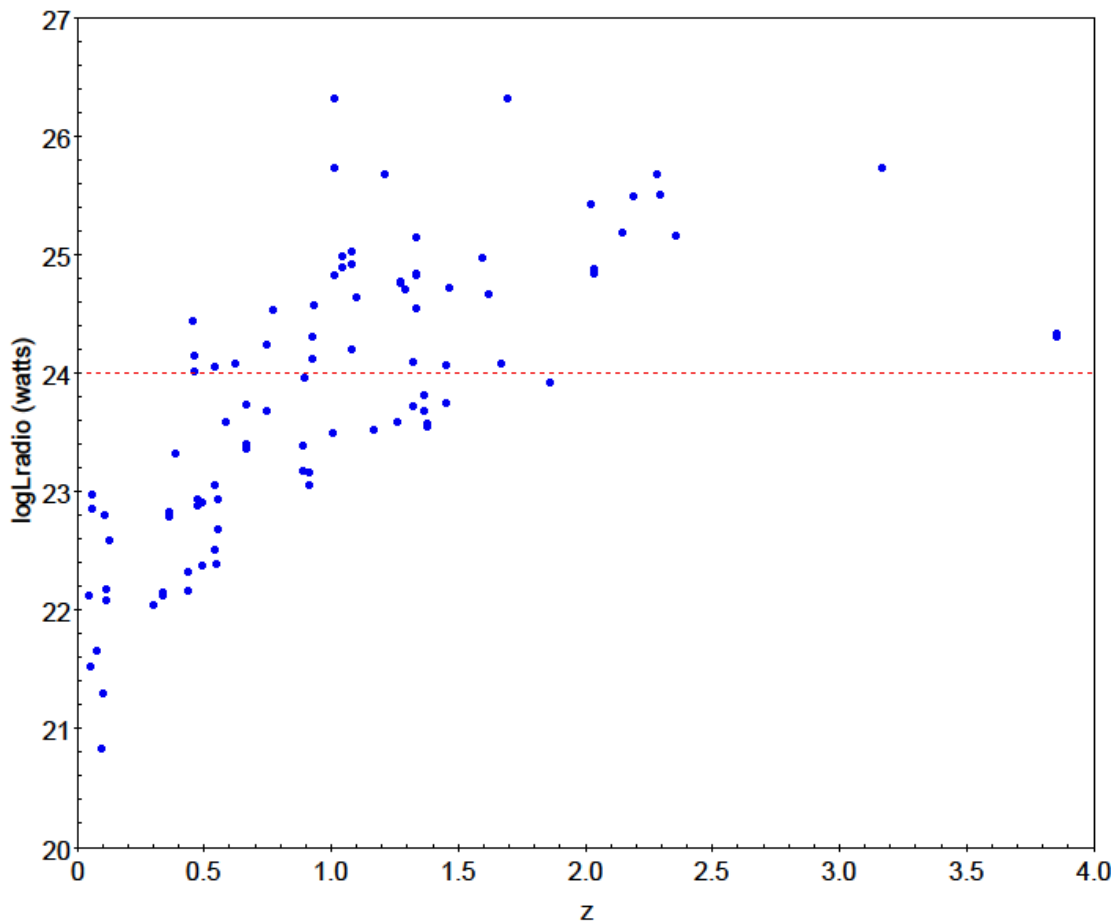


Figure 3.11.-Radio luminosity in watts versus redshift for the 99 detected sources with a radio counterpart.

In order to find the multiwavelength properties of our sources I used some cross-correlation methods separately in the two different areas of the sky.

For the area ELAIS N1 I started with correlating the initial X-ray catalog with the SWIRE catalog and the radio catalogs that are mentioned above. The procedure that I followed started with cross correlating the X-ray catalog with the SWIRE catalog by using a maximum error of 5 arcseconds.

The catalog that was produced by this cross-correlation was an X-ray – Infrared catalog “A” with 410 matches. After that I cross-correlated again with max error of 5 arcseconds the catalog “A” with the VLA FIRST catalog and the NVSS separately, producing a radio –X-ray –Infrared catalog with 9 sources-matches (both cross-correlations with FIRST and NVSS gave the same amount of matches The next step was to use the other radio catalogs that are mentioned above (325-MHz observations of the ELAIS-N1 field, The 610-MHz GMRT Survey of ELAIS-N1 region, The deep VLA 20cm survey) and cross correlate each one of them with the catalog “A”. The final sample from this step was a 32 sources radio-X-ray-Infrared catalog (without the VLA FIRST cross correlation).

Chapter 3 – Sample Selection

For the Lockman Hole area I correlated the SWIRELHCXO-SWIRE/Chandra Lockman Hole Field X-Ray source Catalog with the Ibar-radio Lockman Hole Catalog using 5arcsec error limit and ended up with 59 matches.

To summarize our final catalog by adding of the above matches is, as mentioned, a 501 sources of which of them 402 haven't radio counterparts. For those sources that have very faint radio counterparts we used the limit of 0.75 Jy in the procedure that will be described in the next section. The catalogue contains sources from two different areas of the sky ELAIS N1 and The Lockman Hole. Most of our sources are expected to have an AGN in their core because as mentioned above the cross correlations have been done by using as a base an x-ray data catalog.

Chapter 4

Sample Analysis

In this chapter I am going to analyze our 501 sources sample by dividing it into radio loud and radio quiet populations and investigating if and how these populations depend on galaxy features like the star formation rate and the mass of the host galaxy in the different parts of the electromagnetic spectrum.

4.1 Radio loud- Radio quiet division

In this section I will describe how we divided our sample to the two populations. In order to determine whether the objects are radio loud or radio quiet we used the limit of the radio luminosity R that is described in second chapter. According to Ivezić et al.(2002) b:

$$R_L = \log\left(\frac{f_{radio}}{f_B}\right) = 0.4(M_i - M_{radio})$$

where f_{radio} is defined as the radio flux, f_B is the optical spectral flux in the B band, centered on the wavelength $\lambda=2200 \text{ \AA}$, M_i is the Galactic reddening corrected i-band absolute magnitude (Schlegel et al. 1998) and M_{radio} is the radio flux density at 1.4 GHz converted to the AB system by the following formula (OKE and Gunn,1983):

$$m_{\text{radio}} = -2.5 \log_{10} \left(\frac{f_{1.4\text{GHz}}}{3631\text{Jy}} \right)$$

where $f_{1.4\text{GHz}}$ is the flux density at 1.4 GHz.

Some studies suggest that there is a bimodal distribution in the R parameter for high optical luminosity, high redshift sources (Laor 2003; Ivezić et al. 2004). It has been suggested that even though it is believed that Radio loud and Radio Quiet sources follow the same mechanism of jet production- matter accreting onto the center super massive black hole- they may have a different accretion mode or that their spinning Black Holes have different characteristics. For example they appear to be more massive or spinning faster or even a combination of both (Sikora et al. 2007). Other studies like white et al 2000 declare that there is no evidence of bimodal distribution of radio characteristics in their sample.

In figure 2.2 I mentioned the fact that the results were biased due to the limited observing abilities of our telescopes, however there is a particular distance that we have both QSO and AGN galaxies until the redshift of 1.4 which may be the approximate limit of accurate observations. In the following Figure 4.1 I divide the sources in the two populations.

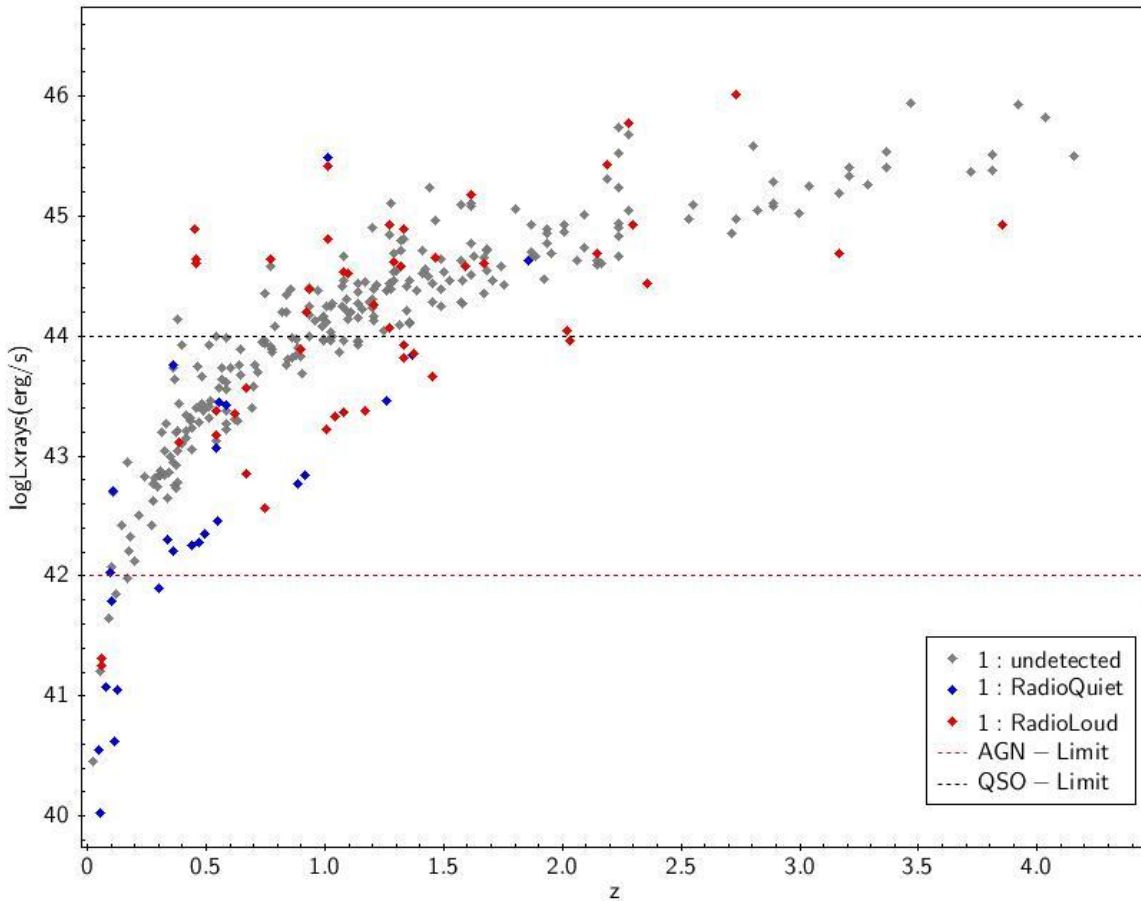


Figure 4.1 .— Redshift versus the logarithm of hard x-ray luminosity. The sources are divided to radio loud with the red color, radio quiet with the blue color. The black line represents the division of starbursts ($L_x < 10^{42}$ erg/s) and AGN ($10^{42} < L_x < 10^{44}$ erg/s). The grey line divides the sources in AGN and QSOs ($L_x > 10^{44}$ erg/s).

The flux limit that I used for our undetected sources is 0.75 mJy, due to the fact that our sources were not able to be traced from the radio telescopes that were used we consider them very faint, thus the majority of them has to be radio quiet objects.

In figure 4.1 we can see that the majority of detected QSOs are radio loud, in the AGN population the radio loud objects have higher luminosities than the radio quiet ones (Figure 4.2). In the histogram of radio loudness in figure 4.3 I divide the whole sample (both detected and undetected sources) in the three populations: starbursts, AGN, QSOs.

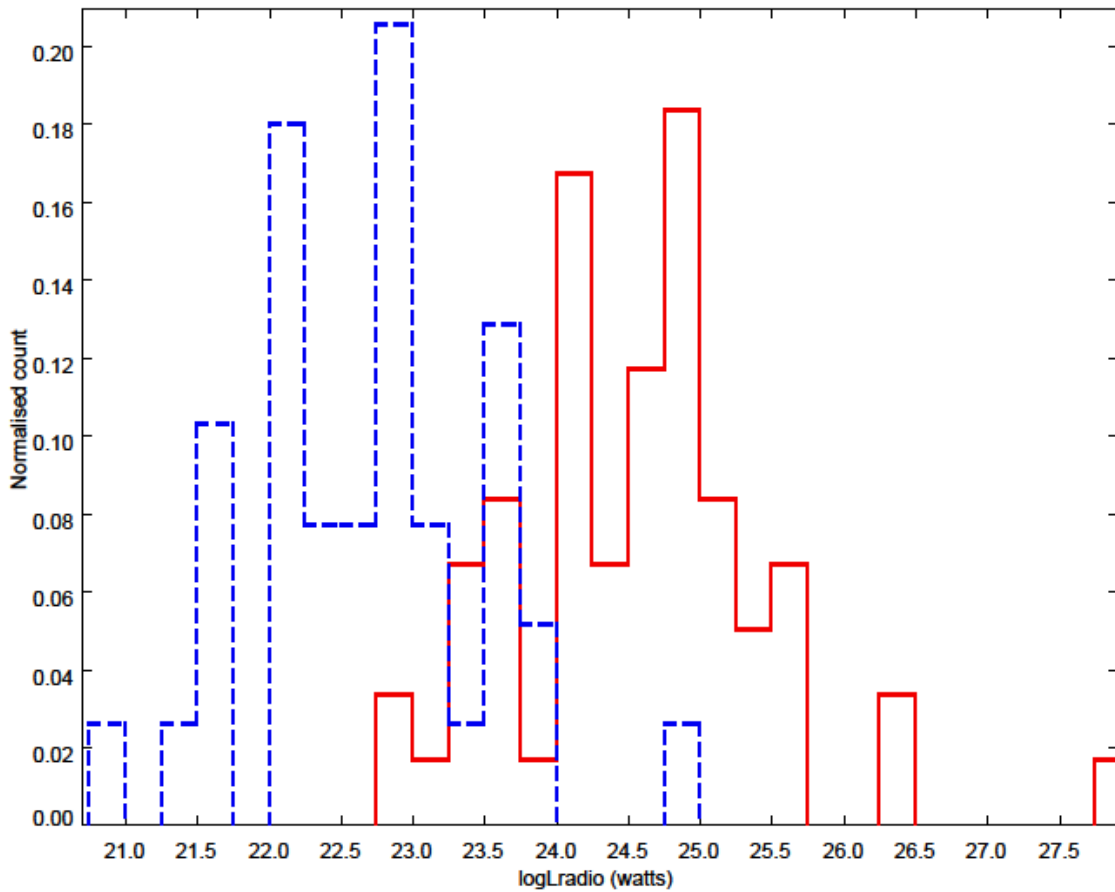


Figure 4.2.- A Histogram of the logarithmic radio luminosity (in watts) of our detected sources. With the red color we represent the radio loud sources of our sample and with the blue dotted line the radio quiet sources.

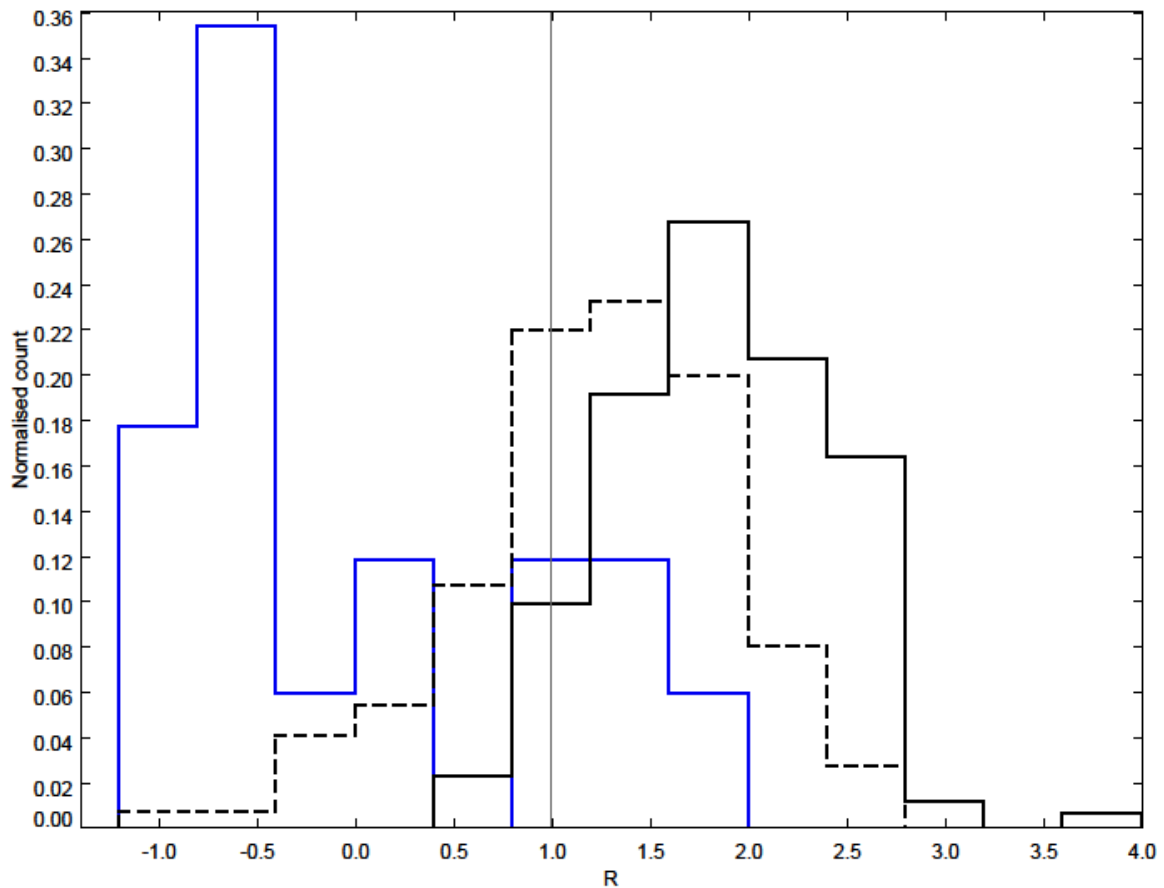


Figure 4.3a.— A histogram of radio loudness. The black line represents the QSO population, the black dotted line the AGN and the blue the starbursts. The grey line is the radio loudness limit, a source with $R < 1$ is radio quiet and a source $R > 1$ is radio loud. In this Histogram we have both radio detected and undetected sources.

In figure 4.3a from the whole 184 QSOs population the 173 are radio loud and the rest 11 are radio quiet objects. This should not surprise us since QSO's are very powerful radio sources. As for the AGN population the 103 from our 151 total number of sources are radio loud and the rest 48 are radio quiet. From the 17 starburst galaxies that we have recognized 5 of them are radio loud sources. In figure 3.3b we can see the exact same histogram but for our detected sample only. From our 36 detected QSOs 34 (94.4%) of them are radio loud. We have 50 apparent AGN sources with a radio component that 23 (46%) of them are categorized as radio loud sources and 27 (54%) of them are radio quiet. For our detected starburst galaxies we have the followings: 2 (16.6%) of our 12 total number of sources are radio loud while the rest are radio quiet.

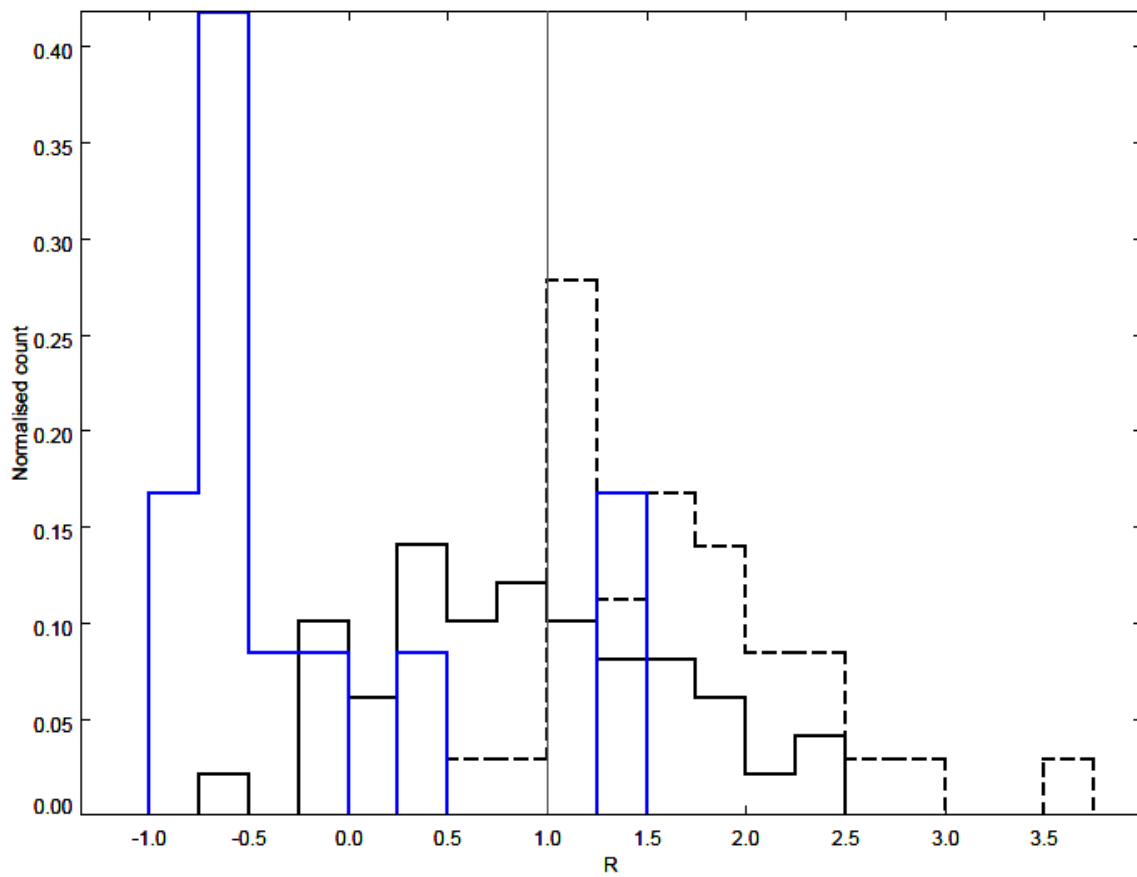


Figure 4.3b.- A histogram of radio loudness. The black line represents the QSO population, the black dotted line the AGN and the blue line the starbursts. The grey line is the radio loudness limit, a source with $R < 1$ is radio quiet and a source $R > 1$ is radio loud. In this Histogram we have only radio detected sources.

4.2 Star Formation Rate

Star formation is galaxy evolution caught in the act. Stars are born in dense molecular gas cocoons that are usually found in the arms of spiral galaxies and the nuclear and circumnuclear regions of the galaxies that are traced within 1-2 kiloparsecs from the galaxy center. The trace of star forming existence is given by the ultraviolet radiation that (mostly OB) stars with star masses greater than ten solar masses can emit. This UV radiation can ionize the hydrogen gas that is found in HII regions of the galaxy, thus the Ha line of the Balmer series in the galaxies spectrum is relatively strong in the optical region. So, some observations that indicate the existence of those star forming galaxies can be the Lyman and Balmer emission lines, their high UV continuum luminosity produced by the hot stars, the infrared thermal emission, the radio continuum emission which is nonthermal, the emission of CO from the molecular clouds and last with the integrated constraints from the total optical luminosity. Many of the properties of galaxies can be understood if we will investigate about their Star Formation Rates (SFR) as suggested by Kennicutt (1983) and Gallagher et al. (1984). The SFR is the rate at which the molecular gas is transformed to stars and it depends on the gas density. According to Condon (1992) and Kennicutt (1998) the following equations are the ones that we used to value the SFR of our sample.

$$SFR = \frac{L_{1.4GHz}}{4.0 * 10^{28}} M_{sun} / yr \quad (1)$$

$$SFR = \frac{L_{FIR}}{2.2 * 10^{43}} M_{sun} / yr \quad (2)$$

where $L_{1.4GHz}$ is the radio luminosity at 1.4 GHz in $erg*s^{-1}*Hz^{-1}$ and L_{FIR} the far infrared luminosity in $erg*s^{-1}$.

For our sample we used the data of the Swire catalog and calculated the star formation rate of our sources by using their far infrared luminosities (equation (2)).

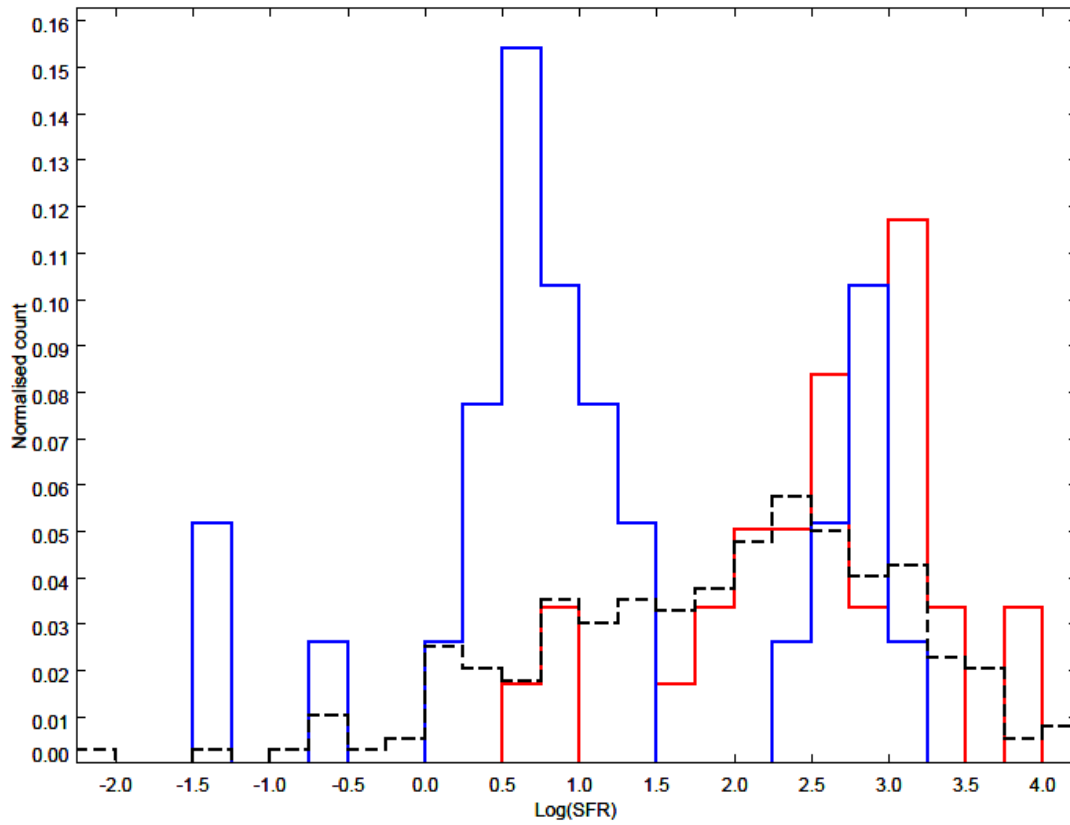


Figure 4.4.-A histogram of the star formation rate in M_{sun}/year . With the black dotted line are shown our undetected sources, the blue represents the radio quiet detected sources and red the radio loud detected sources.

In figure 4.4, a histogram of the star formation rate of our sample, we have 39 radio quiet sources and 60 radio loud. We can see that the radio loud sources of our sample have higher star formation rate which is expected. A radio loud source as mentioned above has much stronger and wider jets than a radio quiet one. There are many theoretical models that suggest that as jets are forming they propagate through host galaxy's dust and they trigger the collapse and fragmentation in many cases of overdense regions that form the star formation cocoons. (Fragile et al.2004; Mellema et al. 2002).

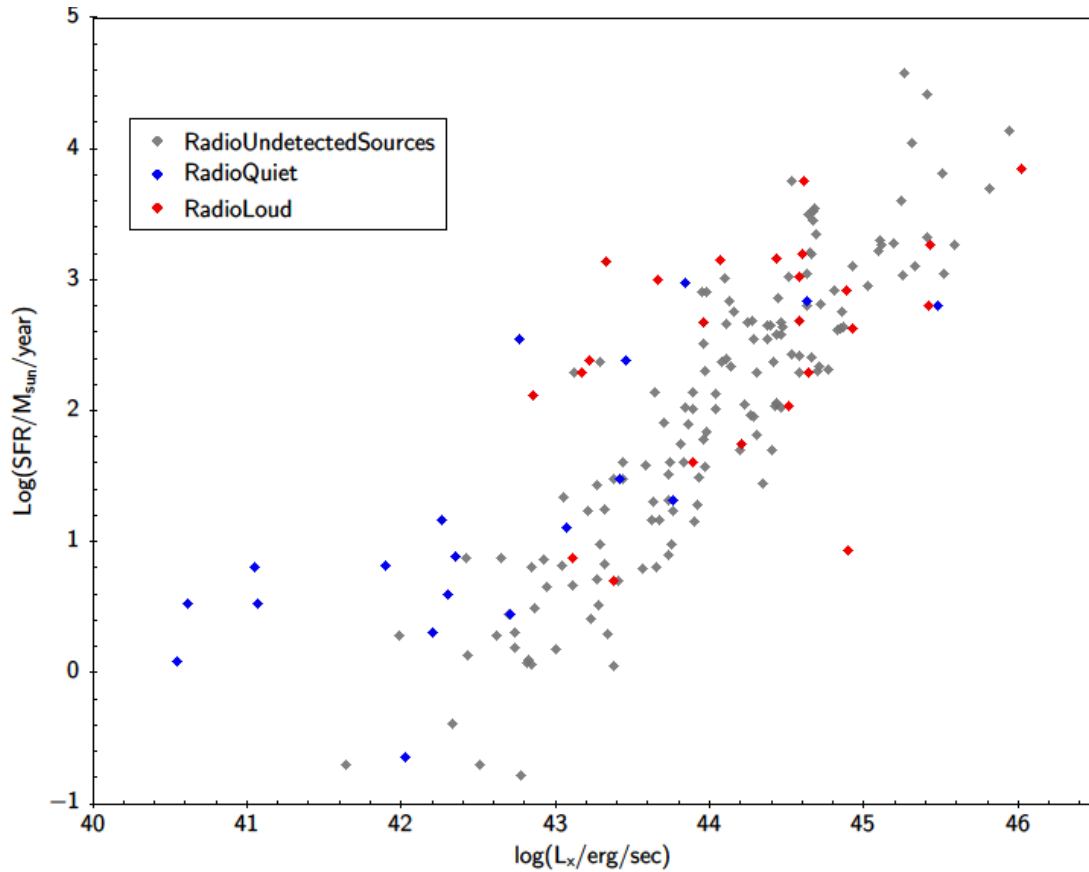


Figure 4.5.- logarithmic star formation rate in $M_{\text{sun}}/\text{year}$ versus logarithmic hard x-ray luminosity in ergs/sec . The red dots represent the radio loud detected sources respectively the blue dots are the detected radio quiet objects and the grey ones are the radio undetected sources of our sample.

As we can see in Figure 4.5 the majority of our radio loud sources have highest hard x-ray luminosity and star formation rate than the radio quiet ones. In this plot we could observe that there is an adequate division of the two population, which is a consistent result to the radio loudness division and to the models that connect strong jets with high star formation that are mentioned in the previous section.

4.3 The Infrared Continuum

The infrared continuum and its origin was a quite major controversy issue due to the fact that even if it couldn't have been thermal it could be produced by the thermal emission from dust grains of the host galaxy. In 1969 Rees with his paper (Rees et al. 1969) gave an answer by suggesting that dust grains heated by ultraviolet and optical emission from the nucleus was the origin of IR emission radiation in Seyferts in the 2.2 – 22 μm . Many years later it had been suggested from multiple research groups that IR emission origin is the UV and optical radiation from the accretion disk by the structural particles of the torus that are graphite-silicate grains (Pier & Krolik 1992; Grabato & Danese 1994; Efstathiou & Rowan-Robinson 1995; Harziminaoglou et al. 2008)

In the following figure 4.6 we can see a histogram of the IR luminosity divided by the optical luminosity so we will avoid of having biased results due to the redshift. The ratio $\frac{L_{ir}}{L_{opt}}$, due to the fact that ir emission is produced by heated interstellar dust, is a measure of the dust opacity of the interstellar medium (Rowan-Robinson et al. 2008)

As we can see in figure 4.6 radio loud sources have higher L_{ir} .

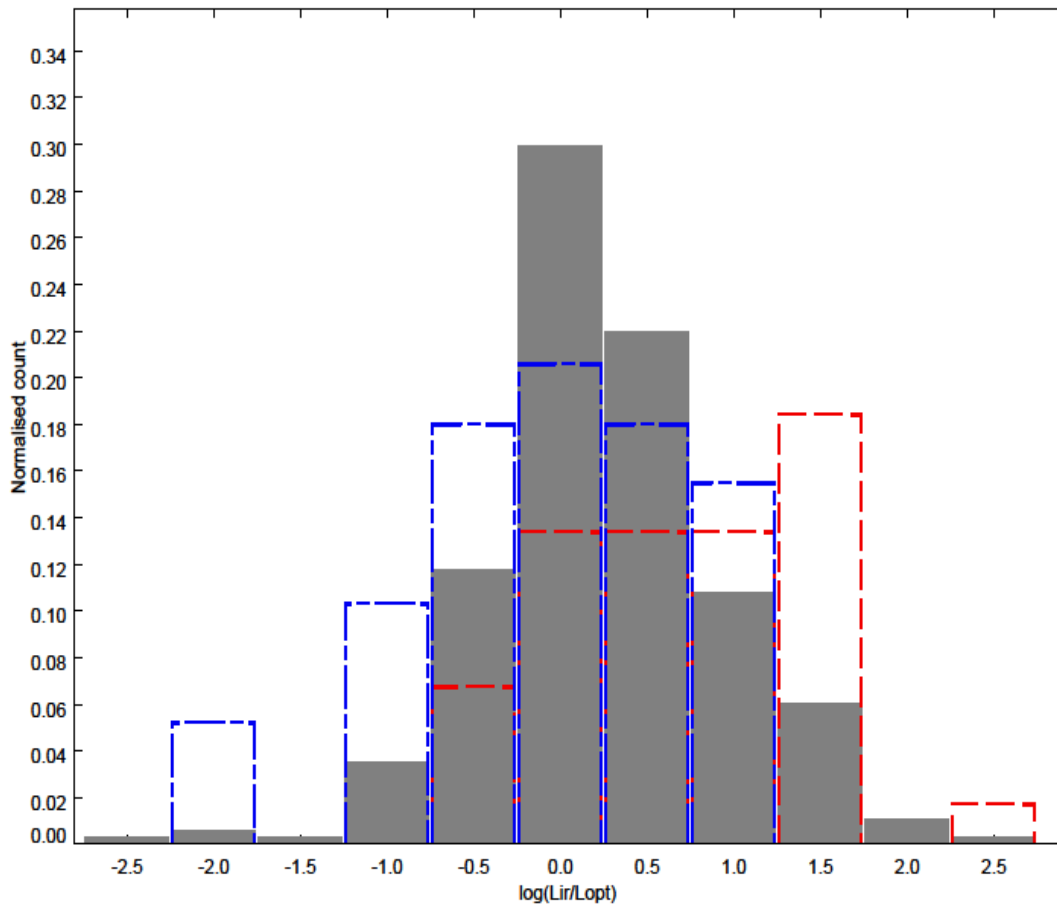


Figure 4.6.- A histogram of the IR luminosity divided by the optical luminosity. Our undetected sample is represented with the grey color, the red shows our detected radio loud sources and respectively the blue corresponds to our detected radio quiet sample.

We used the dust mass from the Swire redshift Catalog in solar units and in Figure 4.7 we present the logarithmic dust mass in solar masses versus the logarithmic star formation masses/year. In 4.8 we present a histogram of the dust mass for the two populations of our sample, radio loud – radio quiet objects. As shown, radio loud objects have higher dust mass than the radio quiet ones. From both 4.7 and 4.8 plots we can make the conclusion that radio loud AGN have dustier host galaxies than radio quiet objects, this may explain the fact that radio loud objects have higher star formation rate too.

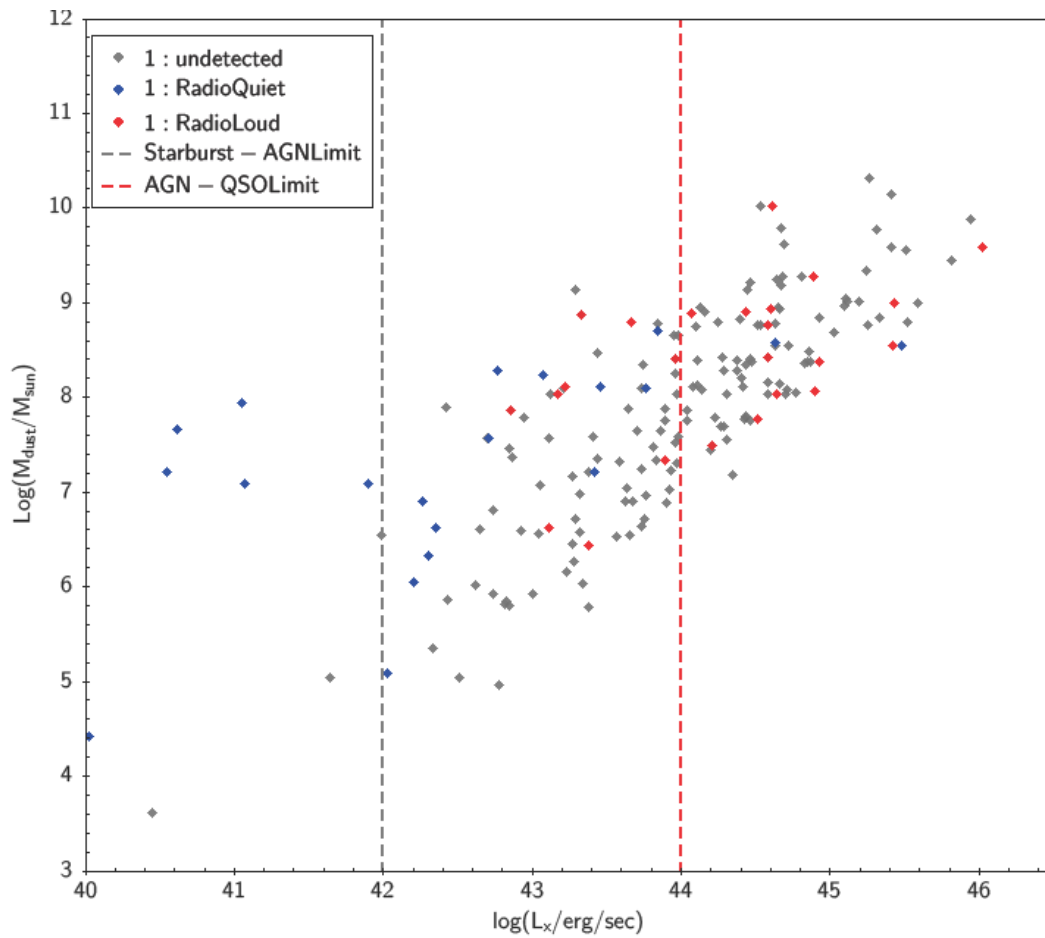


Figure 4.7.- In this figure we present the logarithmic hard X-ray luminosity counted in erg/sec versus the logarithmic M_{dust} counted in M_{sun} (solar masses). With the blue dots we have the radio quiet radio detected sources of our sample accordingly with the red dots.

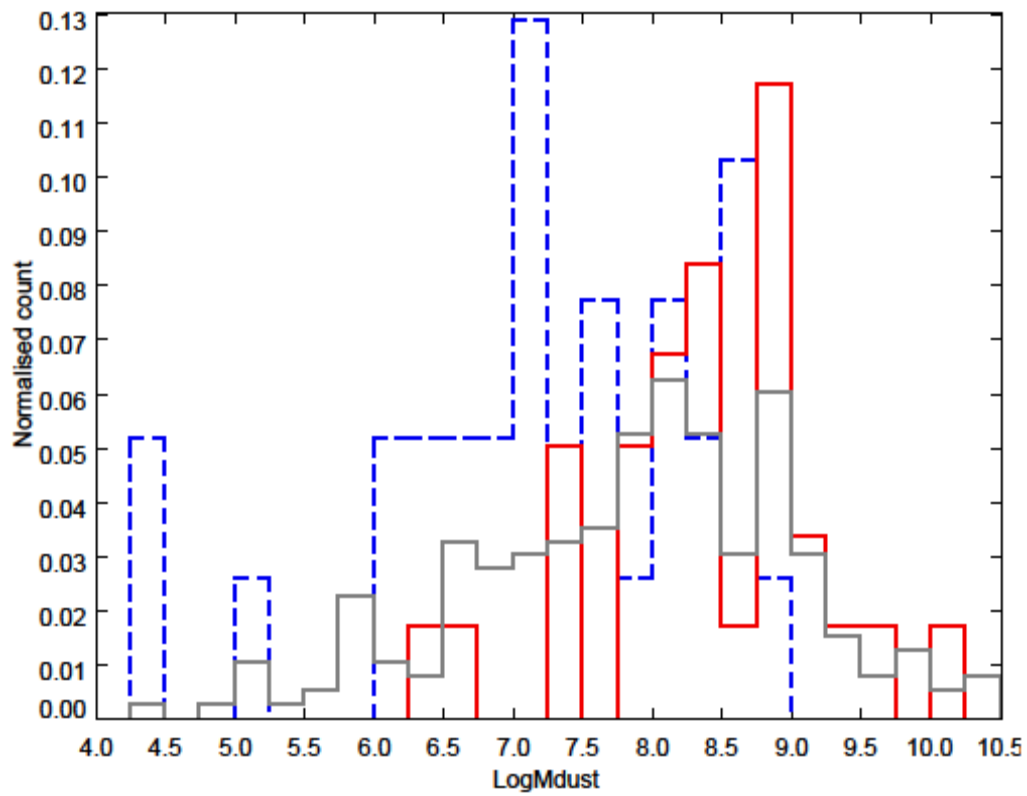


Figure 4.7.- A histogram of the logarithmic dust mass of AGN's host galaxy counted in solar masses. With the blue color we have the radio quiet detected objects of our sample, the red shows the radio loud detected ones and the grey the undetected.

Chapter 5

Results – Conclusions

Simulations of hierarchical structure evolution predict that the black hole growth and AGN activity are associated with the growth of the host galaxy, and that the triggering of the main phase of AGN activity in gas-rich mergers will be accompanied by a major galaxy-wide starburst (Kauffmann and Haehnelt, 2000; Di Matteo et al., 2005; Springel et al., 2005; Hopkins et al., 2008; Somerville et al., 2008). In this section, I discuss the mechanism that may contribute to AGN evolution and the associated star-formation, along with their connection with the presence or not of powerful radio jets.

5.1 Mergers and Triggering of Activity

The early claims that powerful AGN have high incidence of close companions led many studies to suggest a connection between AGN activity, interactions and mergers (e.g. Urrutia et al., 2008; Shankar, 2010; Li et al., 2010; Ramos Almeida et al., 2011). Based on the hierarchical model (e.g., Kauffmann and Charlot, 1998; Kauffmann and Haehnelt, 2000; Di Matteo et al., 2004), the smallest structures were formed first, and SMBHs grew due to major mergers. It has been suggested that major mergers of gas-rich galaxies are an efficient mechanism to feed super massive black holes. For several years, it has been suspected that mergers of galaxies trigger quasar activity (Stockton, 1982; Sanders et al., 1988). This suggestion, is supported by low redshift observed quasars hosts undergoing mergers and interactions (e.g., Canalizo and Stockton, 2001; Kauffmann et al., 2003; Urrutia et al., 2008). Although we note that other deep field studies of the hosts of moderate luminosity AGN have found no significant evidence for high merger rates or interactions (Sanchez et al. 2004) suggesting that secular processes may trigger these AGN. Mergers or inflows of cold gas by other mechanisms not only feed the black hole, but provide a new reservoir of available gas capable of producing a sudden burst of star formation. Based on the scenario of a direct link between mergers and quasars (e.g. Sanders et al. 1988), strong interactions or major mergers between gas-rich galaxies fuel starburst activity and also provide some of the gas for the black hole accretion event.

Major galaxy mergers are also expected to lead to black holes with a high value of spin while minor mergers tend to lead to low values of spin. According to the spin paradigm (Wilson & Colbert 1995) the jet production and power are correlated with the angular momentum of a spinning black hole. The spin paradigm has often been used to explain the radio loudness dichotomy, implying that radio-loud AGN have black holes that spin more than radio-quiet AGN. Based on the above theoretical background, mergers seem to be associated with the AGN activity and the black hole spin which is used to explain the radio loudness dichotomy and maybe the associated star-formation differences between the radio-loud and radio-quiet AGN. One possible explanation is that the high spin black hole produced by the merger powers the radio jets which compress the interstellar gas, triggering star-formation activity during the QSO phase.

5.2 AGN feedback

The physical mechanisms responsible for triggering the active AGN phase are still debated. Indeed, it is still poorly understood whether the AGN activity impacts star formation or vice versa. Negative AGN feedback, where the AGN emission is believed to be responsible for gas heating, is necessary in order to explain the strong suppression of star formation especially in the most massive galaxies (e.g. Croton et al. 2006; Hopkins et al. 2010). The feedback process becomes more complicated in the case of powerful radio sources where there are results that suggest a positive feedback due to the jets inducing star formation in the host galaxy (e.g. Elbaz et al. 2009).

Semi-analytic models invoke AGN feedback to truncate star formation in massive galaxies (e.g. Croton et al. 2006; Bower et al. 2006), often termed negative feedback. This feedback could take several forms such as the photoionizing and heating of the gas reservoirs in the host galaxy (e.g. Pawlik et al. 2009), or the expulsion of significant amounts of gas through outbursts (e.g. Nesvadba et al. 2006). The correlation between the formation of black holes and the star formation can be interpreted in two ways. In the first one, black hole accretion and star formation occur simultaneously because they are both fed from the same gas, brought to the center by gas-rich mergers and disc instabilities. Black hole accretion is then terminated when star formation has used up all the gas. In the second interpretation, star formation terminates when the black hole blows all the gas outside its host galaxy (e.g. Springel et al. 2005; Hopkins et al. 2006a).

Another important aspect of AGN is the role that they play in triggering extensive star formation in a multi-phase intergalactic medium. The same idea has been discussed by several authors concerning the huge expanding radio galaxy lobes, and especially those of the FR II type in order to explain the alignment between large scale optical emission and the axis of their relativistic plasma jets (e.g., McCarthy, 1987; Begelman and Cioffi, 1989; De Young, 1989). The highly relativistic, supersonic jets that power into the surrounding medium and slam into the existing overdensities are able to trigger star formation along cocoons surrounding the jets (e.g. Bicknell et al. 2000; Fragile et al. 2004). This model provides the means of orchestrating star formation over tens of kilo-parsecs on light crossing timescales. This process has been invoked to explain the radio-optical alignment effect at high redshift (Rees 1989).

The different modes of AGN feedback (positive and/or negative) could possibly explain our results for higher star-formation in the case of radio-loud AGN. In figure 5.1 I present the mean star-formation rate values for radio-loud and radio-quiet population with $L_x < 10^{42}$ erg/s (starburst), 10^{42} erg/s $< L_x < 10^{44}$ erg/s (AGN) and $L_x > 10^{44}$ erg/s (quasars). In the case of $L_x < 10^{42}$ erg/s population no radio-loud object is found. This fact is in perfect agreement with the spin paradigm (Blandford, 1990; Wilson and Colbert, 1995) where the jet production and power are correlated with the angular momentum of a rapidly spinning black hole. In the case of AGN with 10^{42} erg/s $< L_x < 10^{44}$ erg/s it seems that radio-loud AGN have on average higher SFR than

radio-quiet AGN with the same X-ray luminosity. This result could be supported by the jet-induced star-formation (positive feedback) idea. Radio jets are able to induce the formation of massive knots of bright young stars, which will disperse and fade over the lifetime of the quasar. However, further study is required in this direction in order to investigate the role of the different type of AGN and if the observed direction affected the radio-loudness and the star-formation rates. At even higher X-ray luminosities ($L_x > 10^{44}$ erg/s) I found no differences between the radio-loud and radio-quiet quasars regarding their SFR. However, I have to notice that there are only 2 radio-quiet quasars detected in radio surveys in our sample and as a result the comparison between the two population is not statistically significant.

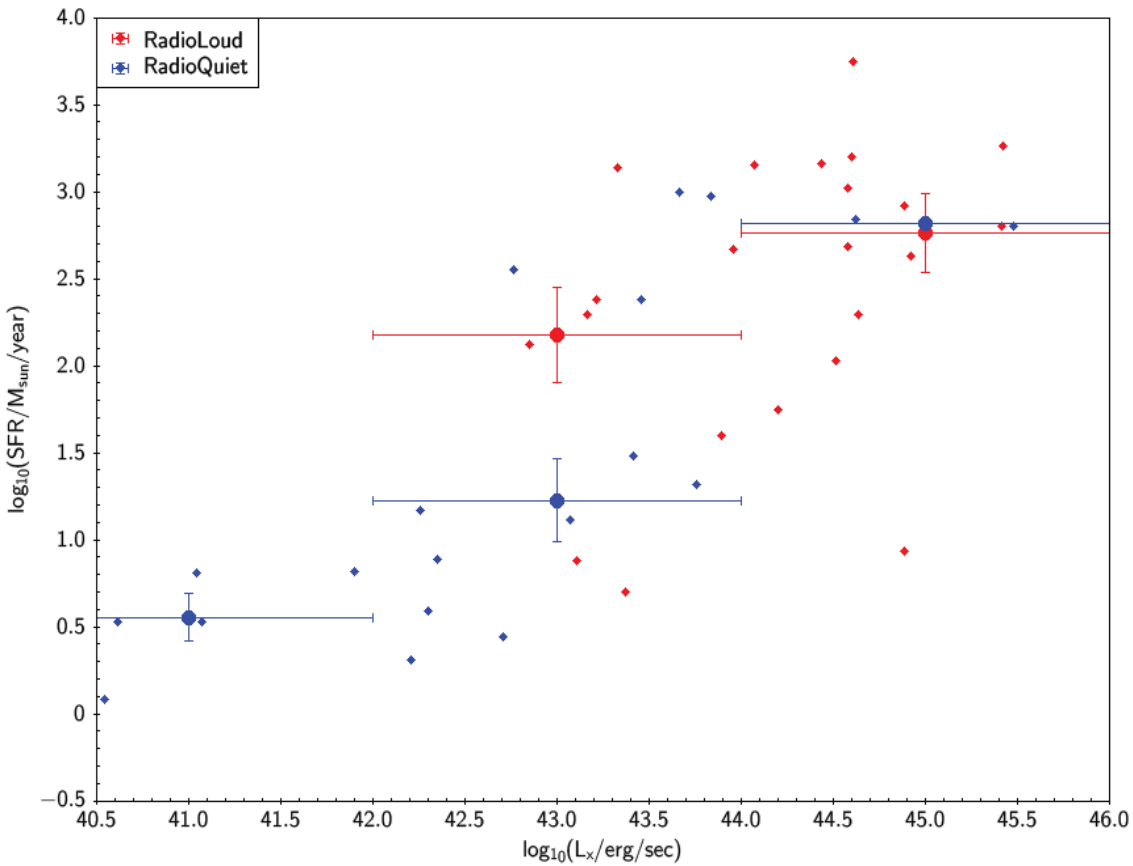


Figure 5.1.-The logarithmic X-ray luminosity in erg/sec versus the logarithmic star formation rate in $M_{\text{sun}}/\text{year}$. With the blue dots we show the radio quiet radio detected sources and with the red ones the radio loud radio detected sources of our sample. With the blue circles we present the mean values of the radio quiet detected sample and with the red circles the mean value of the radio loud detected one. We have placed the mean values in the center of the three classes (starburst, AGN, QSOs). Furthermore with the blue and red straight line we can see the errors.

5.3 Host galaxies

It had been thought based on early samples that powerful radio-loud AGN were hosted by spheroid type galaxies (ellipticals) and radio-quiet AGN were found in disk type galaxies (spirals; e.g. Yee & Green 1984) and this of course provided an obvious suggestion for the reason for their difference. However, as sample sizes have increased they have become more evenly selected and the biases between radio and optical selection have become better understood it now appears that this may not actually be the case. The confusion on this issue had been somewhat affected by the difficulty in studying the host galaxies of luminous QSOs which out-shine their hosts by several magnitudes in some cases.

The host galaxy studies of McLure et al. (1999) and Dunlop et al. (2003) go as far as to show that QSOs brighter than $M_v = -23.5$ (i.e. not Seyferts) are virtually all hosted by spheroidal galaxies. This means that the difference between disk and spheroid hosts is likely related to the mass of the central black hole and not linked directly to the radio power. The apparent link was down to powerful radio-loud AGN being hosted exclusively by the most massive AGN whereas radio-quiet AGN span a much wider range in black hole mass and hence host type. If samples of radio-loud and radio-quiet AGN are selected at random the likelihood is the radio-loud AGN will contain more massive black holes and thus be hosted exclusively in spheroids whereas the sample of RQs will be dominated by the more common lower mass QSOs hosted in spirals.

The relationship between QSOs' optical luminosities and their host galaxy luminosity has also been studied by these works. It might be expected that due to the Magorrian relation the bulge and black hole masses would be closely linked at least at these low redshifts. However, while this might be the case the QSO luminosity as discussed depends also on the accretion rate which has been found to vary significantly. As such although earlier works found some evidence for a correlation between the optical luminosity and the galaxies' brightness the larger and more robust studies of McLure et al. (1999), Dunlop et al. (2003) and Letawe et al. (2010) find at best only a weak relationship.

In Figure 5.2 I present the dust mass of the host galaxy as a function of X-ray luminosity for radio-loud and radio-quiet populations. Similarly to the SFR, radio-loud AGN (10^{42} erg/s $< L_x < 10^{44}$ erg/s) trend to be hosted in galaxies with higher on average dust masses. In the case of quasars, no special differences are found regarding the dust mass of host galaxies in radio-loud and radio-quiet quasar probably due to the lack of radio-detected radio-quiet quasars.

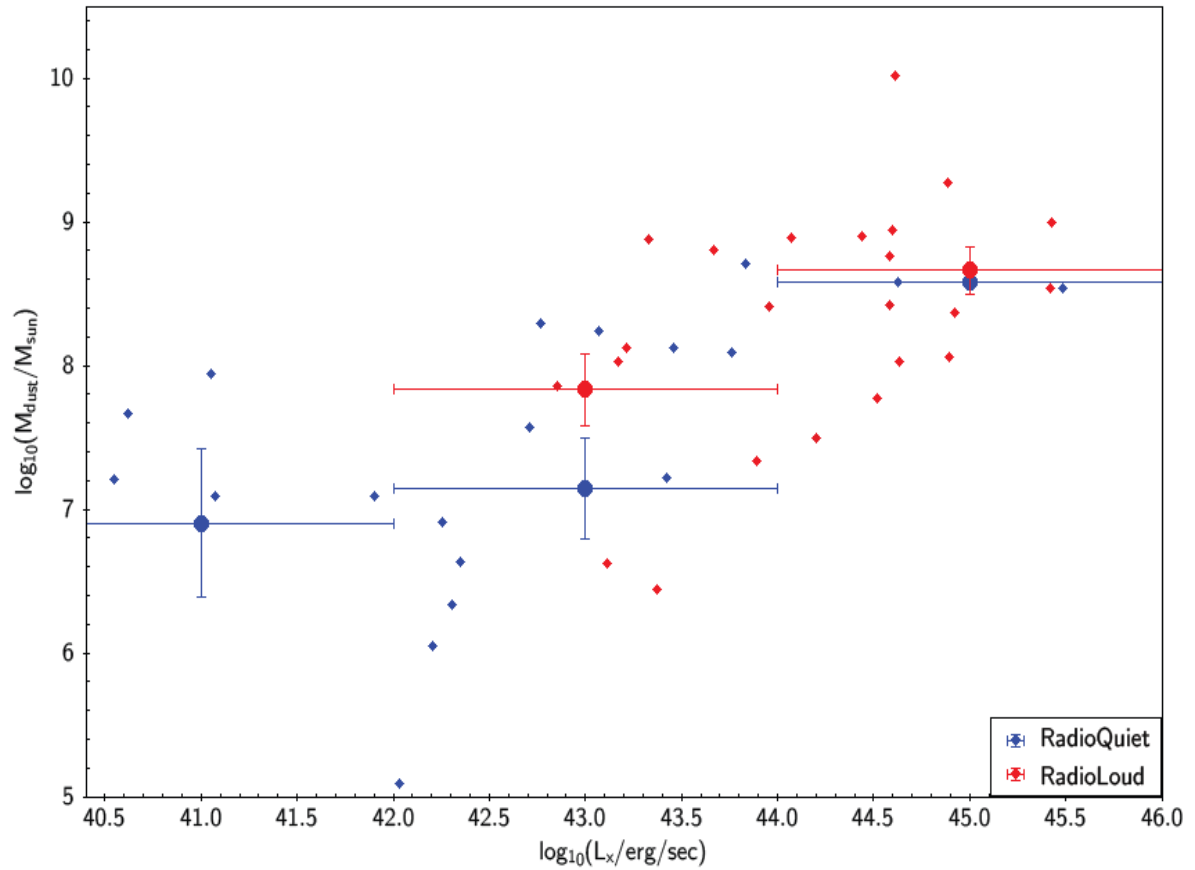


Figure 5.2.-The logarithmic X-ray luminosity in erg/sec versus the logarithmic M_{dust} dust mass of the host galaxy in M_{sun} . With the blue dots we show the radio quiet radio detected sources and with the red ones the radio loud radio detected sources of our sample. With the blue circles we present the mean values of the radio quiet detected sample and with the red circles the mean value of the radio loud detected one. We have placed the mean values in the center of the three classes (starburst, AGN, QSOs). Furthermore with the blue and red straight line we can see the errors.

5.4 Conclusions

In this research project, I obtained a catalog of 501 of starbursts $L_x < 10^{42}$ erg/s, AGN with 10^{42} erg/s $< L_x < 10^{44}$ erg/s and QSO with $L_x > 10^{44}$ erg/s in order to study the relation between radio loud and radio quiet objects. All of our sources had optical, X-rays and infrared counterparts and only 99 sources of our sample had radio counterparts.

Based on their hard X-ray luminosity I investigated the star formation rate of the two populations (RL, RQ) and the dust mass of the host galaxies of our sources. To summarize, the most important conclusions that we can make include that:

- □ There is an absence of radio loud sources in the starburst galaxies of our sample ($L_x < 10^{42}$ erg/s).
- □ There is a tendency for radio loud populations that are divided as AGN (10^{42} erg/s $< L_x < 10^{44}$ erg/s) to have higher star formation rate and higher dust mass.
- □ In QSO object we cannot see a difference between the radio loud and radio quiet population. However this could be a result of the small number of radio quiet sources in our radio detected sample.

References

- A., T. (1974). Gravitational interactions between galaxies.
- A.C. Davenhall, G. P. (16th August 2001). The 2-D CCD Data Reduction Cookbook .
- Almudena Alonso-Herrero, M. P.-S.-G.-S. (September 2009). Local Luminous Infrared Galaxies: Spatially resolved mid-infrared observations with Spitzer/IRS.
- B. T. Soifer, G. N. (2000). High Resolution Mid-Infrared Imaging of Ultraluminous Infrared Galaxies.
- Baldwin, J. A. (February 1981). Classification parameters for the emission-line spectra of extragalactic objects.
- Barnes, J. E. (November 1996). Transformations of Galaxies. II. Gasdynamics in Merging Disk Galaxies.
- Benjamin Robert A., C. E. (August 2003). GLIMPSE. I. An SIRTf Legacy Project to Map the Inner Galaxy.
- Boselli, A. S. (2003). Mid-IR emission of galaxies in the Virgo cluster III. The data .
- Brandl, B. &. *Science with SIRTf - Some Examples*. From Darkness to Light: Origin and Evolution of Young Stellar Clusters, ASP Conference Proceedings, Vol. 243. Edited by Thierry Montmerle and Philippe André. San Francisco: Astronomical Society of the Pacific.
- Brown Robert L., V. B. (December 1991). CO emission at $Z = 2.2867$ in the galaxy IRAS F10214 + 4724.
- C.A.Beichman, G. H. (1988). *Infrared Astronomical Satellite (IRAS) Explanatory Supplement*. NASA.
- C.C. Steidel, K. A. (1999). Lyman Break Galaxies at $z < 4$ and the Evolution of the Ultraviolet Luminosity Density at High Redshift.
- Carico, D. P. (July 1990). The IRAS bright galaxy sample. V - Multibeam photometry of galaxies with L(IR) greater than 10 to the 11th solar luminosities.
- Carol J. Lonsdale, D. F. Ultraluminous Infrared Galaxies. In E. J. Mason, *Astrophysics Update 2 - topical and timely reviews on astronomy and astrophysics* (p. 53). Springer/Praxis books. ISBN: 3-540-30312-X.
- Carol J. Lonsdale, H. E.-R. (August 2003). SWIRE: The SIRTf Wide-area InfraRed Extragalactic Survey.

References

- Carol Lonsdale, M. d.-R. (September 2004). FIRST INSIGHTS INTO THE SPITZER WIDE-AREA INFRARED EXTRAGALACTIC LEGACY.
- Cesarsky, C. J. (November 1996). ISOCAM in flight.
- Chris Pearson (1), H. (. (October 2003). ASTRO-F - Super IRAS - The All Sky Infra-Red Survey.
- Christopher W. Stubbs, P. D. (n.d.). A Method for Extending the Dynamic Range of CCD Instruments.
- Clavel J., S. B. (2000). 2.5-11 micron spectroscopy and imaging of AGNs. Implication for unification schemes.
- Clements D. L., S. W. (March 1996). Optical imaging of ultraluminous IRAS galaxies: how many are mergers?
- Colin J. Lonsdale, P. J. (August 2006). VLBI IMAGES OF 49 RADIO SUPERNOVAE IN ARP 220.
- Colina, L. A. (February 2001). Probable Radio Supernova in NGC 7469.
- Condon, J. J. (1982). Strong radio sources in bright spiral galaxies. II - Rapid star formation and galaxy-galaxy interactions.
- Cs. Kiss, P. A. (2001). Sky Confusion Noise in the Far-Infrared: Cirrus, Galaxies and the Cosmic Far-Infrared Background.
- D. Downes, P. M. (ApJ, 507:615-654). Rotating Nuclear Rings and Extreme Starbursts in Ultraluminous Galaxies. In *November 1998*.
- D. Elbaz, M. A.-F. (November 1992). IRAS 10214 + 4724 - an elliptical galaxy in formation?
- D. Farrah, J. A.-R. (April 2003). Starburst and AGN activity in ultraluminous infrared galaxies.
- D. T. Frayer¹, R. J.-P. (March 1999). Molecular Gas in the $z = 2.565$ Submillimeter Galaxy SMM J14011+0252.
- David Elbaz, C. J. (April 2003). A Fossil Record of Galaxy Encounters.
- DAVID J. SCHLEGEL, D. P. (June 1998). MAPS OF DUST INFRARED EMISSION FOR USE IN ESTIMATION OF REDDENING AND COSMIC MICROWAVE BACKGROUND RADIATION FOREGROUNDS.
- Dean C. Hines, D. E. (February 2006). THE FORMATION AND EVOLUTION OF PLANETARY SYSTEMS (FEPS): DISCOVERY OF AN UNUSUAL DEBRIS SYSTEM ASSOCIATED WITH HD 12039.
- Dopita, L. J. (2002 September). USING STRONG LINES TO ESTIMATE ABUNDANCES IN EXTRAGALACTIC H II REGIONS AND STARBURST GALAXIES.
- Downes D., S. P. (September 1993). Molecular gas mass and far-infrared emission from distant luminous galaxies.
- E. Sturm, D. L. (November 1996). ISO-SWS Spectroscopy of Arp 220 - A highly obscured Starburst Galaxy.
- Edwin, H. (12/1926). Extra-Galactic Nebula.
- EFOSC2 USER'S MANUAL v3.1, Doc. No. LSO-MAN-ESO-36100-0004. (n.d.).
- Efstathiou, M. R.-R. (1993). Multigrain Dust Cloud Models of Starburst and Seyfert Galaxies.
- ELVIS, A. S. (June 1997). Deriving the Quasar Luminosity Function from Accretion-Disk Instabilities.
- ESO. (n.d.). <http://www.eso.org>.
- Fabian., I. M. (March 1991). X-ray reflection from cold matter in active galactic.

References

- Fan, X. e. (2003). A Survey of $z > 5.7$ Quasars in the Sloan Digital Sky Survey. II. Discovery of Three Additional Quasars at $z > 6$.
- Flora M. Li, A. N. (2005). *CCD image sensors in deep-ultraviolet: degradation behavior and damage mechanisms* (Springer ed.). Springer.
- Franceschini A., A. H. (2001). A long-wavelength view on galaxy evolution from deep surveys by the Infrared Space Observatory.
- Francis, P. J. (1991). A high signal-to-noise ratio composite quasar spectrum.
- Frayser, D. T.-P. (October 1998). Molecular Gas in the $z = 2.8$ Submillimeter Galaxy SMM 02399–0136.
- G. G. Fazio, t. I. (September 2004). The Infrared Array Camera (IRAC) For The SPITZER Space Telescope.
- G. H. Rieke, E. T.-C. (September 2004). THE MULTIBAND IMAGING PHOTOMETER FOR SPITZER (MIPS).
- G. Kauffmann, T. M. (December 2003). The host galaxies of active galactic nuclei.
- G.G, F. Infrared Astronomy. In *Frontiers of astrophysics*. Harvard University Press, 1976.
- G.R. Davis, M. G. (November 1996). ISO LWS measurement of the far-infrared spectrum of Saturn.
- Gao, Y. S. (May 2004). The Star Formation Rate and Dense Molecular Gas in Galaxies.
- Gautier T. N. III, B. F. (April 1992). A calculation of confusion noise due to infrared cirrus.
- Helmich, E. v. (August 1996). Infrared absorption of H₂O toward massive young stars.
- Helou, G., & Walker, D. W. (1988). Infrared astronomical satellite (IRAS) catalogs and atlases. Volume 7: The small scale structure catalog.
- Hernquist, L. (August 1989). Tidal triggering of starbursts and nuclear activity in galaxies.
- Hogg, D. W. (1998). The O II Luminosity Density of the Universe.
- Houck, J. R. (n.d.). Early Results from the Infrared Spectrograph on the Spitzer Space Telescope. *The Initial Mass Function 50 years later*. Edited by E. Corbelli and F. Palle, INAF Osservatorio Astrofisico di Arcetri, Firenze, Italy; H. Zinnecker, Astrophysikalisches Potsdam, Germany. *Astrophysics and Space Science Library Volume 327*.
- Howell, S. B. (2000). *Handbook of CCD Astronomy*. Cambridge University Press. <http://www.star.bris.ac.uk/~mbt/topcat/>. (n.d.).
- Impey, C. D. (February 1988). Energy distributions of blazars.
- Ivana Damjanov, M. M. (n.d.). Star Formation Timescales in Spiral Galaxies.
- J. A. Surace, D. S.-S. (August 2005). The SWIRE Data Release 2: Image Atlases and Source Catalogs for ELAIS-N1, ELAIS-N2, XMM-LSS, and the Lockman Hole.
- J.R. Houck, t. S. (September 2004). The Infrared Spectrograph (IRS) on the SPITZER Space Telescope.
- James T. Radomski, R. K. (2003). Resolved Mid-Infrared Emission in the Narrow-Line Region of NGC 4151.
- John Magorrian, S. T. (June 1998). The Demography of Massive Dark Objects in Galaxy Centers.
- JOSEPH, R. D. (n.d.). THE GREAT DEBATE: STARBURSTS AS THE ENERGY SOURCE OF ULTRALUMINOUS INFRARED GALAXIES.

References

- K., H. (1986). An optimal extraction algorithm for CCD spectroscopy.
- K., S. C. (1943). Nuclear Emission in Spiral Nebulae.
- Kennicutt Robert C. Jr., R. K. (May 1987). The effects of interactions on spiral galaxies. II - Disk star-formation rates.
- Kennicutt Robert C. Jr. Armus Lee, B. G. (August 2003). SINGS: The SIRFT Nearby Galaxies Survey.
- Kewley, B. G. (July 2007). Distinguishing Active Galactic Nuclei and Star Formation.
- Kim, S. S.-S. (August 1998). An H I Aperture Synthesis Mosaic of the Large Magellanic Cloud.
- Kinney, D. C. (1992). Lyman-alpha emission in star-forming galaxies - Low-redshift counterparts of primeval galaxies?
- Kleinmann, D. E. (1970). Observations of infrared galaxies.
- Kleinmann, S. G.-W. (May 1988). The properties and environment of the giant, infrared-luminous galaxy IRAS 09104 + 4109.
- Kormendy, J. &. (May 1992). Ultraluminous IRAS galaxies - Formation of elliptical galaxies by merger-induced dissipative collapse.
- Krolik, J. H. (1999). *Active galactic nuclei: from the central black hole to the galactic environment*. Princeton University Press.
- L. C. Ho, A. V. (October 1997). Properties of H II Regions in the Centers of Nearby Galaxies.
- Larsen, S. S. (May 29, 2009). IRAF notes for Observational Astrophysics I.
- Laurent, O. M. (2000). Mid-infrared diagnostics to distinguish AGNs from starbursts.
- Leech K. J., R.-R. M. (March 1994). Optical structure of a large sample of ultraluminous IRAS galaxies.
- Leitherer, C. (2001). Time Scales in Starbursts.
- Lemaitre, G. R. (2008). *Astronomical Optics and Elasticity Theory: Active Optics Methods*. Springer.
- Lemke D., K. U.-P. (November 1996). ISOPHOT - capabilities and performance.
- Linda Siobhan Sparke, J. S. (2007). *Galaxies in the universe: an introduction*. Cambridge University Press.
- Lisa A. Wells, D. J. (September 13, 1994). Cleaning Images of Bad Pixels and Cosmic Rays Using IRAF.
- Lisa J. Kewley, B. G. (May 2006). The Host Galaxies and Classification of Active Galactic Nuclei.
- Longair, M. S. (1996). *Our evolving universe*. CUP Archive.
- Lonsdale C.J, P. S. (1984). INFRARED OBSERVATIONS OF INTERACTING/MERGING GALAXIES .
- Low J., K. D. (November 1968). Proceedings of the Conference on Seyfert Galaxies and Related Objects: 17. Infrared Observations of Seyfert Galaxies, Quasistellar Sources, and Planetary Nebulae.
- Lutz, D. (March 1999). ISO observations of the Galactic Centre.
- Lynden-Bell, D. (1969). Galactic Nuclei as Collapsed Old Quasars.
- M. Bolzonella, J.-M. M. (2000.). Photometric redshifts based on standard SED fitting procedures.
- M. Lacy, L. J.-L. (2004). Obscured and Unobscured Active Galactic Nuclei in the Spitzer Space Telescope First Look Survey.

References

- M. Rowan-Robinson, T. B. (2008). Photometric redshifts in the SWIRE Survey.
- M. W. Werner, T. L. (September 2004). The Spitzer Space Telescope Mission.
- M.F. Kessler, J. S. (August 1996). The Infrared Space Observatory (ISO) Mission.
- M.J. Sawicki, H. L. (1997). Evolution of the Galaxy Population Based on Photometric Redshifts in the Hubble Deep Field.
- M. Werner, G. G. (June 2006). First Fruits of the Spitzer Space Telescope: Galactic and Solar System Studies.
- Madau, P. (1999). In S. S. Holt and E. P. Smith eds, *After the Dark Ages: When Galaxies Were Young*.
- Madau, P. (1995). Radiative transfer in a clumpy universe: The colors of high-redshift.
- Magorrian John, T. S. (June 1998). The Demography of Massive Dark Objects in Galaxy Centers.
- Maraston, C. (2005). Evolutionary population synthesis: models, analysis of the ingredients and application to high-z galaxies.
- Mason, J. W. (2004). *Astrophysics Update 2, Topical and Timely Reviews of Astrophysics*. Springer.
- Massey, P. (Feb 1997). A User's Guide to CCD Reductions with IRAF.
- Massey, P. (February 1997). A User's Guide to CCD Reductions with IRAF.
- Matsuhara H., W. T. (May 2006). Deep Extragalactic Surveys around the Ecliptic Poles with AKARI (ASTRO-F).
- Mihos, J. C. (June 1996). Gasdynamics and Starbursts in Major Mergers.
- Miley, G. K. (June 1985). IRAS observations of Seyfert galaxies.
- Mirabel, D. B. (1996). LUMINOUS INFRARED GALAXIES.
- Mirabel, I. F. (1988). 21 centimeter survey of luminous infrared galaxies.
- Modern CCD Detectors for Spectroscopy and Imaging. (November 2003). *LoT Oriel Group Europe*.
- N.M. Ball, J. L. (2004). Galaxy types in the Sloan Digital Sky Survey using supervised artificial neural networks.
- Nakagawa, T. ASTRO-F Survey As Input Catalogues For FIRST. In J. A. G.L.Pilbratt, *The Promise of the Herschel Space Observatory*. ESA SP-460.
- Nancy Remeig Evans, E. B.-V.-W. (February 1998). Classical Cepheid Masses: U Aquilae.
- NASA. (n.d.). <http://www.ipac.caltech.edu>.
- Neal J. Evans II, L. E. (August 2003). FROM MOLECULAR CORES TO PLANET-FORMING DISKS: A SIRTf LEGACY.
- Neugebauer, G. H., & Boggess, N. C. (March 1984). The Infrared Astronomical Satellite (IRAS) mission.
- Neugebauer, G. M. (September 1986). Quasars measured by the Infrared Astronomical Satellite.
- NOAO. (n.d.). <http://iraf.noao.edu>.
- O. Le Fevre, D. C. (December 1995.). The Canada-France Redshift Survey. II. Spectroscopic Program: Data for the 0000-00 and 1000+25 Fields. *ApJ*, 455:60.
- P.E. Clegg, P. A.-P.-C. (October 1996). The ISO Long-Wavelength Spectrometer.
- P.M. Solomon, S. R. (March 1992). Molecular gas content of the primaeval galaxy IRAS 10214 + 4724.
- P.Vaisanen, E. G. (n.d.). Confusion limit due to galaxies: using SIRTf's Infrared Array Camera.

References

- Phil Massey, F. V. (April 1992). A User's Guide to Reducing Slit Spectra with IRAF.
- Pierre Léna, F. L. (1998). *Observational astrophysics*. Springer.
- Privett, G. (2007). Image Reduction. In *Creating and Enhancing Digital Astro Images*. Springer.
- Puget, J.-L. A.-P.-X. (April 1996). Tentative detection of a cosmic far-infrared background with COBE.
- Puget, J.-L. L. (1985). Contribution of large polycyclic aromatic molecules to the infrared emission of the interstellar medium.
- Pullen, A. C. (14 June 2003). The Zen of IRAF, A Spiritual User's Guide to the "Image Reduction and Analysis Facility" for the LINUX Novice.
- R. Genzel, D. L.-G. (May 1998). What Powers Ultraluminous IRAS Galaxies?
- R. S. Furuya, S. T. (December 10, 2008). Subaru Data Reduction Cookbook: Grism Spectroscopic Observations with IRCS.
- Rees, M. (1984). Black Hole Models for Active Galactic Nuclei.
- Richards, G. T.-M. (2001). Quasar Absorption Lines as a Function of Quasar Orientation Measures.
- Rieke, G. H., & Low, F. J. (1972). Infrared Photometry of Extragalactic Sources.
- Rigopoulou, D. S. (December 1999). A Large Mid-Infrared Spectroscopic and Near-Infrared Imaging Survey of Ultraluminous Infrared Galaxies: Their Nature and Evolution.
- Robinson T. F., G. M. (1988). Coiled perimysial fibers of papillary muscle in rat heart: morphology, distribution, and changes in configuration.
- Robinson, K. (2007). *Spectroscopy: the key to the stars, reading the lines in stellar spectra*. Springer.
- Rocca-Volmerange, D. L. (2002). Photometric redshifts from evolutionary synthesis with PEGASE: The code Z-PEG and the $z=0$ age constraint.
- Rowan Robinson, M. (1999). The star-formation history of the universe.
- Rowan-Robinson, M. (1995). A new model for the infrared emission of quasars.
- Rowan-Robinson, M. (n.d.). A Submillimeter Survey of the Hubble Deep Field - Implications for the Star Formation History of the Universe.
- Rowan-Robinson, M. e. (June 1991). A high-redshift IRAS galaxy with huge luminosity - Hidden quasar or protogalaxy?
- Rowan-Robinson, M. (August 2000). Hyperluminous infrared galaxies.
- Rowan-Robinson, M. (May 1987). Models for infrared emission from IRAS galaxies.
- Rowan-Robinson, M. (2003). Photometric redshifts in the Hubble Deep Fields: evolution of extinction and the star formation rate.
- Rowan-Robinson, M. (2003.). Quantifying dust and the ultraviolet radiation density in the local Universe.
- Sanders D.B., M. I. (September 1996). Luminous Infrared Galaxies.
- Sanders, D. B. (January 1986). Massachusetts-Stony Brook Galactic plane CO survey. I - (b,V) maps of the first Galactic quadrant.
- Sanders, D. B. (1988). Ultraluminous infrared galaxies and the origin of quasars.
- Sanders, D. S. (February 1988). Ultraluminous infrared galaxies and the origin of quasars.
- Sarajedini, V. L. (2003). THE NATURE OF LOW LUMINOSITY ACTIVE GALAXIES AT $Z \sim 1$.

References

- Saunders W., R.-R. M. (January 1990). The 60-micron and far-infrared luminosity functions of IRAS galaxies.
- Schechter, P. (1976). An analytic expression for the luminosity function for galaxies.
- Schneider, P. (2006). 3. The World of Galaxies. In *Extragalactic astronomy and cosmology: an introduction*. Springer.
- Scoville, M. S. (November 1998). CO (J = 4 → 3) and 650 Micron Continuum Observations of the z = 0.93 Hyperluminous Infrared Galaxy FSC 15307+3252.
- Shupe David L., R.-R. M. (November 2007). GALAXY COUNTS AT 24 MICRONS IN THE SWIRE FIELDS.
- Slipher, V. M. (1917). The spectrum and velocity of the nebula N.G.C. 1068 (M 77).
- Smith, H. E. (2002). Infrared Surveys for AGN.
- Soifer B. T., N. G.-R. (August 1984). The remarkable infrared galaxy ARP 220 = IC 455.
- Soifer B. T., S. D. (September 1987). The IRAS bright galaxy sample. II - The sample and luminosity function.
- Solomon P.M, S. L. (1988). STAR-FORMATION RATES, MOLECULAR CLOUDS, AND THE ORIGIN OF THE FAR-INFRARED LUMINOSITY OF ISOLATED AND INTERACTING GALAXIES.
- Solomon, P. M. (March 1997). The Molecular Interstellar Medium in Ultraluminous Infrared Galaxies.
- Stiavelli, M. (2009). *From First Light to Reionization: The End of the Dark Ages*. Wiley-VCH.
- Surace, J. A. (February 1999). High-Resolution Tip/Tilt Near-Infrared Imaging of Warm Ultraluminous Infrared Galaxies.
- Surace, J. A. (January 1998). HST/WFPC2 Observations of Warm Ultraluminous Infrared Galaxies.
- Szczerba Ryszard, S. G. (February 2003). Classification of ISO SWS01 spectra of proto-planetary nebulae: a search for precursors of planetary nebulae with [WR] central stars.
- T. S. R. Babbedge, M. R.-R.-S.-F. (2004). ImpZ: a new photometric redshift code for galaxies and quasars.
- T. S. R. Babbedge, M. R.-R.-S.-F. (2004). ImpZ: a new photometric redshift code for galaxies and quasars.
- T. S. R. Babbedge, M. R.-R.-S.-F. (May 2006). Luminosity functions for galaxies and quasars in the Spitzer Wide-Area Infrared Extra-galactic (SWIRE) Legacy survey.
- T.W.B. Muxlow, R. B. (September 2006). Starburst Galaxies. *PoS(8thEVN)031* .
- Takahara, Y. Y. (1988). Galactic evolution and cosmology - Probing the cosmological deceleration parameter.
- Team, M. D. (January 2005). The Great Observatories Origins Deep Survey (GOODS) Spitzer Legacy Science Program.
- Technology, I. b. (page 137, August 2007). Chapter 7 : Infrared Spectrograph (IRS). In *Spitzer Space Telescope Observer's Manual – Version 8.0*.
- Tennyson, J. (2005). *Astronomical spectroscopy: an introduction to the atomic and molecular physics of astronomical spectra*. Imperial College Press.

References

- Th. de Graauw, T. H. (1996). Observing with the ISO Short-Wavelength Spectrometer.
- Th. Encrenaz, T. d.-S. (November 1996). First results of ISO-SWS observations of Jupiter.
- Theo Koupelis, K. F. (2007). Light and the Electromagnetic Spectrum. In *In Quest of the Universe*. Jones & Bartlett Publishers.
- TIMOTHY M. HECKMAN, C. R. (August 1998). The Ultraviolet Spectroscopic Properties of Local Starbursts: Implications at High Redshift.
- Toomre, A. (1977). in *Evolution of Galaxies and Stellar Populations*, p. 401.
- Tran, Q. D., Lutz, D., Genzel, R., Rigopoulou, D., Spoon, H. W., Sturm, E., et al. (May 2001). ISOCAM-CVF 5-12 MICRON SPECTROSCOPY OF ULTRALUMINOUS INFRARED GALAXIES.
- Trichas, M. (2008). Multi-Wavelength Surveys of Extreme Infrared Populations.
- V. Charmandaris, O. L. (1999). The Mid-IR view of interacting galaxies.
- Veilleux, S. S.-C. (July 1997). A Near-Infrared Search for Hidden Broad-Line Regions in Ultraluminous Infrared Galaxies.
- Wei Zheng, G. A. (1997). A Composite HST Spectrum of Quasars.
- Xu C., L. C. (April 2003). Models for Evolution of Dusty and E/S0 Galaxies Seen in Multiband Surveys.
- Y. Wang, N. B. (1998). A Catalog of Color-based Redshift Estimates for $Z < 4$ Galaxies in the Hubble Deep Field.
- York, D. A. (2000). THE SLOAN DIGITAL SKY SURVEY: TECHNICAL SUMMARY.